ISSN: 2153-1196 Volume 12, Number 1, January 2021

Scientific Research Publishing

Journal of Modern Physics

Special Issue on Quantum Physics and Its Applications

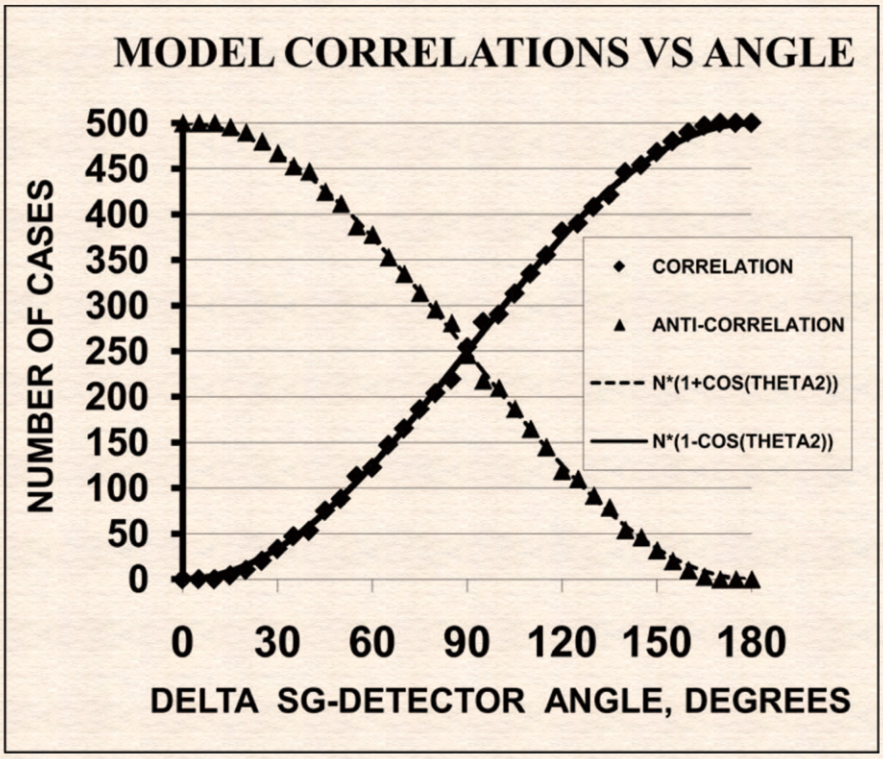

ISSN: 2153-1196
9 772153 119007 01

https://www.scirp.org/journal/jmp

Journal Editorial Board

ISSN: 2153-1196 (Print) ISSN: 2153-120X (Online)
https://www.scirp.org/journal/jmp

Editor-in-Chief

Editorial Board

Journal of Modern Physics, 2021, 12, 1-58
https://www.scirp.org/journal/jmp
ISSN Online: 2153-120X
ISSN Print: 2153-1196

Table of Contents

Volume 12 Number 1 January 2021

The figure on the front cover is from the article published in Journal of Modern Physics, 2021, Vol. 12, No. 1, pp. 50-58 by Kenneth H. Schatten.

Journal of Modern Physics (JMP)
Journal Information

SUBSCRIPTIONS

The *Journal of Modern Physics* (Online at Scientific Research Publishing, https://www.scirp.org/) is published monthly by Scientific Research Publishing, Inc., USA.

Subscription rates:
Print: $89 per issue.
To subscribe, please contact Journals Subscriptions Department, E-mail: sub@scirp.org

SERVICES

Advertisements
Advertisement Sales Department, E-mail: service@scirp.org

Reprints (minimum quantity 100 copies)
Reprints Co-ordinator, Scientific Research Publishing, Inc., USA.
E-mail: sub@scirp.org

COPYRIGHT

PRODUCTION INFORMATION

For manuscripts that have been accepted for publication, please contact:
E-mail: jmp@scirp.org

Journal of Modern Physics, 2021, 12, 1-9
https://www.scirp.org/journal/jmp
ISSN Online: 2153-120X
ISSN Print: 2153-1196

Transient Quantum Beat Oscillations in Extreme-Relativistic Diffraction in Time

Salvador Godoy

Universidad Nacional Autónoma de México, Facultad de Ciencias, Física, CDMX, Coyoacán, México
Email: sgs@ciencias.unam.mx

How to cite this paper: Godoy, S. (2021) Transient Quantum Beat Oscillations in Extreme-Relativistic Diffraction in Time. *Journal of Modern Physics*, **12**, 1-9.
https://doi.org/10.4236/jmp.2021.121001

Received: November 24, 2020
Accepted: January 3, 2021
Published: January 6, 2021

Abstract

In the solution of the Klein-Gordon equation for the shutter problem, we prove that, at internuclear distances, a relativistic beam of Pi-mesons has a probability density which oscillates in time in a similar way to the spatial dependence in optical Fresnel diffraction from a straight edge. However, for an extreme-relativistic beam, the Fresnel oscillations turn into quantum damped beat oscillations. We prove that quantum beat oscillations are the consequence, at extreme-relativistic velocities, of the interference between the initial incident wave function, and the Green's function in the relativistic shutter problem. This is a pure quantum relativistic phenomenon.

Keywords

Quantum Beat Oscillations, Relativistic Diffraction in Time

1. Introduction

Quantum beat oscillations are a common subject in Atomic and Molecular Spectroscopy. In Atomic physics, the term quantum beat refers to a superposed oscillatory behavior in the light intensity emitted by some suddenly excited atomic systems in their subsequent decay [1]. In Molecular Spectroscopy, quantum beat spectroscopy is a Doppler-free time domain method based on the creation of molecular coherences with a laser pulse and the measurement of their subsequent time evolution [2].

In this same context is the work of Villavicencio *et al.* [3], where transient phenomena of phase-modulated cutoff wave packets were explored by deriving an exact general solution to Schrödinger's equation for finite-range potentials involving arbitrary initial quantum states. They show that the dynamical features of the probability density are governed by a virtual two-level system. They also

found that for a system with a bound state the interplay between the virtual levels with the latter causes a quantum beat. They also find a regime characterized by a time-diffraction oscillation. This last result came as a big surprise; it happens that in the exact Schrödinger's solution of the shutter problem [4], where we find diffraction in time as a consequence of the free time-evolution of an initial space-discontinuous beam of particles, the exact analytic expression for the probability density has a structure in which quantum beats do not exist.

Diffraction in time oscillations is a pure quantum phenomenon, and similar oscillations arise at the moment of closing and opening gates in nanoscopic circuits [5]. With adequate potentials added to the model, it has been used to study transient dynamics of tunneling matter waves [6], and the transient response to abrupt changes of the interaction potential in semiconductor structures and quantum dots [7]. For a review on the subject see [8] [9]. There is, in summary, a strong motivation for a thorough understanding of transient time oscillation of beams of matter.

In this paper we address the following question: are there quantum shutter solutions (not in the Schrödinger's equation) where quantum beats substitute the usual Fresnel oscillations of diffraction in time? In this paper, we report the positive finding of such result in the diffraction in time of an extreme-relativistic beam of free particles.

The main contribution of this paper is to show the existence of transient quantum beats in the extreme-relativistic quantum shutter problem. After solving the Klein-Gordon equation for the 1D shutter problem, we prove that, at internuclear distances, a relativistic beam of neutral Pi-mesons, has a probability density which oscillates in time in a similar way to the Fresnel oscillations derived in the Schrödinger equation. However, for an extreme-relativistic beam, the Fresnel oscillations turn into quantum damped beats!

2. The Klein-Gordon Shutter Problem

In the relativistic shutter problem for spin-0 particles, we assume for all $t \le 0$, that we have a discontinuous right-moving plane wave in the left side of a perfectly absorbing shutter, and zero to the right:

$$\psi(x, t \le 0) = \begin{cases} \mathrm{e}^{i(kx-\omega t)} & x \le 0 \\ 0 & x > 0 \end{cases} = \mathrm{e}^{i(kx-\omega t)}\theta(-x), \tag{1}$$

here $\theta(x)$ denotes the step function, and the angular frequency is given by $\omega = c\left(k^2 + \mu^2\right)^{1/2}$ and $\mu \equiv mc/\hbar$. At $t = 0$, when the shutter is suddenly opened, we have the initial conditions:

$$\psi(x, 0) = \mathrm{e}^{ikx}\theta(-x), \quad \frac{\partial \psi(x, 0)}{\partial t} = -i\omega \mathrm{e}^{ikx}\theta(-x), \tag{2}$$

which we use to solve the Klein-Gordon (K-G) equation,

$$\frac{\partial^2 \psi}{\partial x^2} - \frac{\partial^2 \psi}{\partial (ct)^2} = \mu^2 \psi. \tag{3}$$

The *exact* solution of this initial-value problem is given in the appendix A, where we use dimensionless variables for "position" χ and "time" τ defined by

$$\chi \equiv \mu x = \frac{mc}{\hbar} x, \quad \tau \equiv \mu ct = \frac{mc^2}{\hbar} t. \tag{4}$$

For arbitrary ($\tau > 0$, $\chi > 0$), on the right-hand side of the shutter, we have the *exact* K-G wave function solution:

$$\begin{aligned} \frac{2\mathrm{e}^{i\Omega\tau}}{\theta(\tau-\chi)}\psi(\chi,\tau;\Omega) &= \mathrm{e}^{i\Omega\chi} - \int_{\chi}^{\tau} \mathrm{d}u\, \mathrm{e}^{i\Omega u} \left\{ \chi \frac{J_1\left[\xi(\chi,u)\right]}{\xi(\chi,u)} + i\kappa J_0\left[\xi(\chi,u)\right] \right\} \\ &\equiv \mathrm{e}^{i\Omega\chi} + i\kappa\left(C_0 + iS_0\right) - \chi\left(C_1 + iS_1\right). \end{aligned} \tag{5}$$

Here, we have defined both dimensionless "wave-number" κ and "angular-frequency" Ω as:

$$\xi(\chi,\tau) \equiv \sqrt{\tau^2 - \chi^2}, \quad \kappa \equiv \frac{k}{\mu} = \frac{v/c}{\sqrt{1-(v/c)^2}}, \quad \Omega \equiv \frac{\omega}{\mu c} = \frac{1}{\sqrt{1-(v/c)^2}}. \tag{6}$$

We have also defined, the real functions: (C_0 , S_0 , C_1 , S_1) given by:

$$C_0(\chi,\tau;\Omega) + iS_0(\chi,\tau;\Omega) \equiv \theta(\tau-\chi)\int_{\chi}^{\tau} \mathrm{e}^{i\Omega u} J_0\left[\xi(\chi,u)\right]\mathrm{d}u, \tag{7a}$$

$$C_1(\chi,\tau;\Omega) + iS_1(\chi,\tau;\Omega) \equiv \theta(\tau-\chi)\int_{\chi}^{\tau} \mathrm{e}^{i\Omega u} \frac{J_1\left[\xi(\chi,u)\right]}{\xi(\chi,u)}\mathrm{d}u. \tag{7b}$$

3. Time-Dependent Density

Given the K-G wave function $\psi(x,t)$, the probability density is calculated by:

$$\rho(x,t) = \frac{i\hbar}{2mc^2}\psi^* \frac{\partial\psi}{\partial t} + c.c., \tag{8}$$

which, for dimensionless variables, turn into $\rho(\chi,\tau)$, we have:

$$\rho(\chi,\tau) = \frac{i}{2}\psi^*(\chi,\tau)\frac{\partial\psi(\chi,\tau)}{\partial\tau} + c.c. \tag{9}$$

Notice that the initial relativistic plane-wave, $\psi(\chi,\tau\le 0) = \exp\left[i(\kappa\chi - \Omega\tau)\right]$, does not have unit density, in fact we have

$$\rho(\chi,\tau\le 0) = \Omega. \tag{10}$$

This means, as we will show, that the time-evolved density $\rho(\chi>0,\tau>0)$ will oscillate in time around the initial value: $\rho = \Omega$. Using Equation (5) we get for arbitrary ($\tau > 0$, $\chi > 0$) the *exact* K-G probability density:

$$\begin{aligned} &\frac{8\rho(\chi,\tau)}{\Omega\theta(\tau-\chi)} \\ &= \left[\mathrm{e}^{i\Omega\chi} - \chi\left(C_1 + iS_1\right) - i\kappa\left(C_0 + iS_0\right) - i\frac{\chi}{\Omega}\frac{J_1(\xi)}{\xi}\mathrm{e}^{i\Omega\tau} + \frac{\kappa}{\Omega}J_0(\xi)\mathrm{e}^{i\Omega\tau} \right] \\ &\times\left[\mathrm{e}^{-i\Omega\chi} - \chi\left(C_1 - iS_1\right) + i\kappa\left(C_0 - iS_0\right) \right] + c.c. \end{aligned} \tag{11}$$

The presence of the function $\theta(\tau-\chi)$ implies, as expected, that for times $0 \le t \le x/c$ the density vanishes, in full agreement with the relativity theory.

4. Relativistic Diffraction in Time for Pi-Mesons

At this point, we apply our present results to a relativistic beam of neutral Pi-mesons (π^0) which are 0-spin particles. We know that Pi-mesons are the carriers of nuclear forces and for this, and no other reason, we assume a particle detector fixed at a distance x from the shutter of about, $x = 1.7\times10^{-15}\,\text{m}$, where nuclear forces have a maximum range. All mesons are unstable and decay in various ways. Neutral Pi-mesons have a mean-life given by: $t^0 \approx 10^{-17}\,\text{sec}$, which for a mass of, $m = 135\ \text{MeV}/\text{c}^2$, we have, $\tau^0 \approx 10^{+7}$. Consequently, our theoretical predictions for diffraction in time for neutral Pi-mesons will make sense only if the predicted transient behavior happens in a range of times $\Delta\tau$ having orders of magnitude less than τ^0. Next, we will show that for all assumed conditions of position and energy, this condition is well satisfied.

Let us assume a relativistic beam of monochromatic, $\omega = c\left(k^2+\mu^2\right)^{1/2}$, $\mu \equiv mc/\hbar$, neutral Pi-mesons ($m = 135\ \text{MeV}/\text{c}^2$) with "low" velocities, $v/c = 0.5$, and a particle detector at, $x = 1.7\times10^{-15}\,\text{m}$. Using the exact result in Equation (12) we show in **Figure 1** the plot of the relativistic probability density versus time.

The main features of this plot are: 1) As expected, for times $0 \le t \le x/c$ the density vanishes. 2) In spite of the fact that the exact relativistic density given in Equation (12) looks different from the Schrödinger one, however, for $t > x/c$ the damped oscillations we see in **Figure 1** look similar to the ones predicted in the optical Fresnel diffraction by a straight edge [10]. We claim that diffraction in time is present in relativistic quantum mechanics! 3) We measure the period of one initial oscillation, $\Delta\tau = 41$, which corresponds to $\Delta t = 2\times10^{-22}\,\text{sec}$! This range is well below the π^0 -meson's mean-life: $t^0 \approx 10^{-17}\,\text{sec}$.

5. Damped Beats in Extreme-Relativistic Diffraction in Time

The next obvious question is: how does diffraction in time look like for extreme-

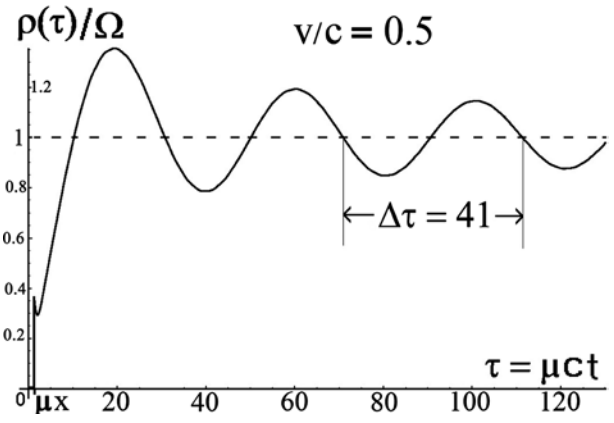

Figure 1. Relativistic diffraction in time of Pi-mesons, $v/c = 0.5$.

relativistic values of v/c? In this section, we show properties of extreme relativistic diffraction in time which, as far as we know, have never been reported before.

As we gradually increase the relativistic velocities v/c, the diffraction in time pattern gradually changes from Fresnel into damped beats! To illustrate this, in Figure 2, we have chosen the particular case of an extreme-relativistic beam of neutral Pi-mesons, $v/c = 0.99$. Assuming the particle detector at a fixed distance, $x = 1.7\times10^{-15}\,\mathrm{m}$, we plot as a function of time the K-G shutter density $\rho(\chi,\tau)$, given in Equation (12). We clearly see the gradual distorsion of the Fresnel oscillatios.

Finally in Figure 3 for a more energetic beam, $v/c = 0.998$, we clearly see the total transformation of the Fresnel oscillations into a perfect case of quantum beats. Here for the slow, modulating amplitude, we measure its period: $\Delta\tau_{slow} = 6$, which means a "slow" oscillation with a modulating period, $T_{slow} = 3\times10^{-23}\,\mathrm{sec}$ and an angular frequency $\omega_{slow} = 2\times10^{+23}\,\mathrm{sec}^{-1}$. As for the fast oscillations we have $\Delta\tau_{fast} = 0.4$, implying a shorter period, $T_{fast} = 2\times10^{-24}\,\mathrm{sec}$ and a faster angular frequency: $\omega_{fast} = 3\times10^{+24}\,\mathrm{sec}^{-1}$. All periods are shorter than the π^0 -meson's mean-life: $t^0 \approx 10^{-17}\,\mathrm{sec}$.

6. Conclusions

Two simultaneous properties are needed for the existence of quantum beats. The

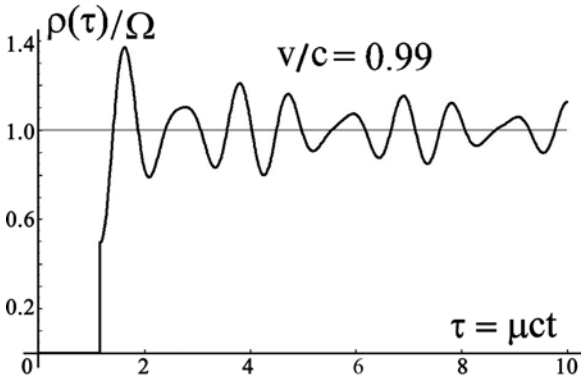

Figure 2. Deformed Fresnel oscillations for extreme relativistic Pi-mesons.

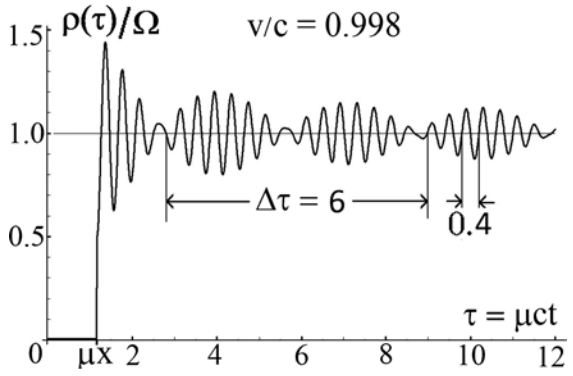

Figure 3. Transient quantum beats for extreme relativistic Pi-mesons.

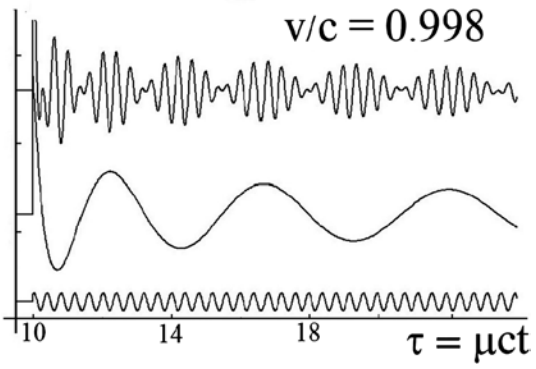

Figure 4. From bottom to top: the trigonometric, the Bessel, and the product.

first is that in the probability density, which is a quadratic expression of the wave function, we have products of two different oscillatory functions. In our case in Equation (12) we have the most important contribution of these products:

$$\left[\sin(\Omega\tau)+\cos(\Omega\tau)\right]J_0\left(\sqrt{\tau^2-\chi^2}\right)\quad(\tau\geq\chi) \tag{12}$$

where the agular frequency Ω is given by $\Omega\equiv\dfrac{1}{\sqrt{1-(v/c)^2}}$.

The second property is that only for extreme relativistic velocities the two oscillatory functions must have similar angular frequencies. Here, for $v/c=0.998$, ($\Omega=15$), the Bessel J_0 becomes a slow oscillating function of time and each trigonometric is a fast one. See **Figure 4**. The products show damped beats! However, for $v/c<0.9$, the beats are no longer present.

In conclusion, quantum beat oscillations are the consequence, at extreme relativistic velocities, of the interference between the initial incident wave function: $e^{i\Omega\tau}$, and the Green's function of the relativistic shutter problem: $J_0\left(\tau^2-\chi^2\right)$. This a pure quantum relativistic phenomenon. We claim that our result is original and has never been reported before.

A. The Klein-Gordon Solution for the 1D Shutter Problem

Let us consider the Klein-Gordon (K-G) equation for $\psi(\chi,\tau)$ defined in the infinite range $-\infty<\chi<\infty$,

$$\frac{\partial^2\psi}{\partial\chi^2}-\frac{\partial^2\psi}{\partial\tau^2}=\psi. \tag{13}$$

We demand bounded boundary conditions: $\lim_{|x|\to\infty}\left|\psi(\chi,\tau)\right|<\infty$, and the initial conditions, corresponding to the shutter problem:

$$\psi(\chi,0)=e^{i\kappa\chi}\theta(-\chi),\quad\frac{\partial\psi(\chi,0)}{\partial\tau}=-i\Omega e^{i\kappa\chi}\theta(-\chi) \tag{14}$$

where $\Omega\equiv\sqrt{1+\kappa^2}$.

To solve the K-G equation, we begin taking the Laplace transform of Equation (14). Denoting,

$$\phi(\chi,s)\equiv\mathcal{L}\left[\psi(\chi,\tau)\right]\equiv\int_0^\infty \mathrm{e}^{-s\tau}\psi(\chi,\tau)\,\mathrm{d}\tau,$$

we find the differential equation

$$\frac{\mathrm{d}^2\phi(\chi,s)}{\mathrm{d}\chi^2}-\left(s^2+1\right)\phi(\chi,s)=-\left(s-i\Omega\right)\mathrm{e}^{i\kappa\chi}\theta(-\chi) \tag{15}$$

which holds in the range $-\infty<\chi<\infty$.

Due to the presence of the step function $\theta(-\chi)$, the origin $\chi=0$ is a singular point where the function and its first derivative must be continuous. This fact suggests to break the infinite range into the left ($\chi\le 0$) and right ($\chi\ge 0$) ranges, having different differential equation for each one. For the left-hand side of the shutter, $\chi\le 0$, we define $\phi_<(\chi,s)$ as the solution of the differential equation:

$$\frac{\mathrm{d}^2\phi_<}{\mathrm{d}\chi^2}-\left(s^2+1\right)\phi_<=-\left(s-i\Omega\right)\mathrm{e}^{i\kappa\chi}, \tag{16}$$

and for the right-hand side, $\chi\ge 0$, we define $\phi_>(\chi,s)$ as the solution of

$$\frac{\mathrm{d}^2\phi_>}{\mathrm{d}\chi^2}-\left(s^2+1\right)\phi_>=0. \tag{17}$$

Here both functions $\phi_<$ and $\phi_>$ must be bounded: ($\phi_<$ at $\chi\to-\infty$) and ($\phi_>$ at $\chi\to+\infty$). The important boundary condition is that the two functions and their corresponding first derivatives must be continuous at the interface, $\chi=0$.

Equations (17) and (18) are ordinary second order differential equations and their solution is readily obtained. Taking into account the boundary conditions at $\pm\infty$ we have:

$$\phi_<(\chi,s)=A\mathrm{e}^{\chi\sqrt{s^2+1}}+\frac{1}{s+i\Omega}\mathrm{e}^{i\kappa\chi}\quad(\chi\le 0) \tag{18}$$

and

$$\phi_>(\chi,s)=B\mathrm{e}^{-\chi\sqrt{s^2+1}}\quad(\chi\ge 0) \tag{19}$$

The constants A and B are fixed from the continuity conditions at the interface $\chi=0$:

$$\phi_<(0,s)=\phi_>(0,s),\quad \mathrm{d}\phi_<(0,s)/\mathrm{d}\chi=\mathrm{d}\phi_>(0,s)/\mathrm{d}\chi$$

We have a set of coupled algebraic equations for the constants A and B:

$$A+\frac{1}{s+i\Omega}=B \tag{20}$$

$$A\sqrt{s^2+1}+\frac{i\kappa}{s+i\Omega}=-B\sqrt{s^2+1} \tag{21}$$

with solutions given by:

$$2A=\frac{-1}{s+i\Omega}\left(1+\frac{i\kappa}{\sqrt{s^2+1}}\right) \tag{22}$$

$$2B = \frac{1}{s+i\Omega}\left(1-\frac{i\kappa}{\sqrt{s^2+1}}\right) \tag{23}$$

Substituting Equation (23) into Equation (19) and Equation (24) into Equation (20) we get, in space (χ, s), the *exact* solution for relativistic diffraction in time.

For $(\chi \le 0)$ we have the solution:

$$\phi_<(\chi,s) = \frac{-1}{2}\frac{1}{s+i\Omega}\left(1+\frac{i\kappa}{\sqrt{s^2+1}}\right)e^{\chi\sqrt{s^2+1}} + \frac{1}{s+i\Omega}e^{i\kappa\chi}, \tag{24}$$

and for $(\chi \ge 0)$ we have:

$$\phi_>(\chi,s) = \frac{1}{2}\frac{1}{s+i\Omega}\left(1-\frac{i\kappa}{\sqrt{s^2+1}}\right)e^{-\chi\sqrt{s^2+1}}. \tag{25}$$

To get the time solution in the variable τ, we must invert the Laplace transforms. We readily find in Laplace Transforms Tables [11] the following results.

$$\mathcal{L}^{-1}\left[\frac{1}{s+i\Omega}\right] = e^{-i\Omega\tau} \tag{26}$$

$$\mathcal{L}^{-1}\left[e^{-|\chi|\sqrt{s^2+1}}\right] = \delta(\tau-|\chi|) - |\chi|\frac{J_1\left(\sqrt{\tau^2-\chi^2}\right)}{\sqrt{\tau^2-\chi^2}}\theta(\tau-|\chi|) \tag{27}$$

$$\mathcal{L}^{-1}\left[\frac{e^{-|\chi|\sqrt{s^2+1}}}{\sqrt{s^2+1}}\right] = J_0\left(\sqrt{\tau^2-\chi^2}\right)\theta(\tau-|\chi|) \tag{28}$$

where $J_0(x)$ and $J_1(x)$ denote Bessel functions. Next, using the convolution theorem, and after some simplifications we have:

$$\mathcal{L}^{-1}\left[\frac{e^{-|\chi|\sqrt{s^2+1}}}{(s+i\Omega)\sqrt{s^2+1}}\right] = \theta(\tau-|\chi|)\int_{|\chi|}^{\tau} du\, e^{-i\Omega(\tau-u)}J_0\left(\sqrt{u^2-\chi^2}\right) \tag{29}$$

and

$$\mathcal{L}^{-1}\left[\frac{e^{-|\chi|\sqrt{s^2+1}}}{s+i\Omega}\right] = \theta(\tau-|\chi|)\left[e^{-i\Omega(\tau-|\chi|)} - |\chi|\int_{|\chi|}^{\tau} du\, e^{-i\Omega(\tau-u)}\frac{J_1\left(\sqrt{u^2-\chi^2}\right)}{\sqrt{u^2-\chi^2}}\right] \tag{30}$$

With the help of Equations (30) and (31) we have the final solutions:

For $\chi \le 0$ we get, as expected, the incident and reflected wave:

$$\begin{aligned}\psi_<(\chi,\tau) = e^{i(\kappa\chi-\Omega\tau)} - \frac{1}{2}\theta(\tau+\chi)\Bigg[&e^{-i\Omega(\chi+\tau)} + \chi\int_{-\chi}^{\tau} du\, e^{i\Omega(u-\tau)}\frac{J_1\left(\sqrt{u^2-\chi^2}\right)}{\sqrt{u^2-\chi^2}} \\ &+ i\kappa\int_{-\chi}^{\tau} du\, e^{i\Omega(u-\tau)}J_0\left(\sqrt{u^2-\chi^2}\right)\Bigg],\end{aligned} \tag{31}$$

and for $\chi \ge 0$ we get the transmitted wave:

$$\psi_{>}(\chi,\tau)=\frac{1}{2}\theta(\tau-\chi)\left[\mathrm{e}^{i\Omega(\chi-\tau)}-\chi\int_{\chi}^{\tau}\mathrm{d}u\,\mathrm{e}^{-i\Omega(\tau-u)}\frac{J_1\left(\sqrt{u^2-\chi^2}\right)}{\sqrt{u^2-\chi^2}}\right.$$
$$\left.-i\kappa\int_{\chi}^{\tau}\mathrm{d}u\,\mathrm{e}^{-i\Omega(\tau-u)}J_0\left(\sqrt{u^2-\chi^2}\right)\right], \tag{32}$$

We see that in fact, the 1D shutter problem is nothing but a particular time-dependent scattering problem, and here we have the exact relativistic solution.

Conflicts of Interest

The author declares no conflicts of interest regarding the publication of this paper.

References

[1] Hegerfeldt, G.C. and Plenio, M.B. (1994) *Quantum Optics*: *Journal of the European Optical Society Part B*, **6**, 15. https://doi.org/10.1088/0954-8998/6/1/003

[2] Carter, R.E. and Huber, J.R. (2000) *Chemical Society Reviews*, **29**, 305-314. https://doi.org/10.1039/a900724e

[3] Villavicencio, J. and Hernández-Maldonado, A. (1996) *Physical Review A*, **54**, 3055. https://doi.org/10.1103/PhysRevA.101.042109

[4] Moshinsky, M. (1951) *Physical Review*, **84**, 525. https://doi.org/10.1103/PhysRev.84.525

[5] Schneble, D., Hasuo, M., Anker, T., Pfau, T. and Mlynek, J. (2003) *Journal of the Optical Society of America B*, **20**, 648-651. https://doi.org/10.1364/JOSAB.20.000648

[6] Brouard, M. and Muga, J.G. (1996) *Physical Review A*, **54**, 3055. https://doi.org/10.1103/PhysRevA.54.3055

[7] Delgado, F., Cruz, H. and Muga, J.G. (2002) *Journal of Physics A*: *Mathematical and General*, **35**, 1037. https://doi.org/10.1088/0305-4470/35/48/311

[8] Garca-Calderón, G., Rubio, G. and Villavicencio, J. (1999) *Physical Review A*, **59**, 1758. https://doi.org/10.1103/PhysRevA.59.1758

[9] Delgado, F., Muga, F., Ruschhaput, A., Garca-Calderón, G. and Villavicencio, J. (2003) *Physical Review A*, **68**, Article ID: 032101. https://doi.org/10.1103/PhysRevA.68.032101

[10] Born, M. and Wolf, E. (1965) Principles of Optics. Pergamon Press, Oxford.

[11] Abramowitz, M. and Stegun, I.A. (1965) Handbook of Mathematical Functions. Dover Publications, New York.

Journal of Modern Physics, 2021, 12, 10-21
https://www.scirp.org/journal/jmp
ISSN Online: 2153-120X
ISSN Print: 2153-1196

Bell Correlations from Local Un-Entangled States of Light and Quantum Electro-Dynamics

Louis Sica[1,2]

[1]Institute for Quantum Studies, Chapman University, Orange, CA & Burtonsville, MD, USA
[2]Inspire Institute Inc., Alexandria, VA, USA
Email: lousica@jhu.edu

How to cite this paper: Sica, L. (2021) Bell Correlations from Local Un-Entangled States of Light and Quantum Electro-Dynamics. *Journal of Modern Physics*, **12**, 10-21.
https://doi.org/10.4236/jmp.2021.121002

Received: November 21, 2020
Accepted: January 5, 2021
Published: January 8, 2021

Abstract

Based on the Bell theorem, it has been believed that a theoretical computation of the Bell correlation requires explicit use of an entangled state. Such a physical superposition of light waves occurs in the down-converter sources used in Bell experiments. However, this physical superposition is eliminated by wave propagation to spatially separated detectors. Bell correlations must therefore result from local waves, and the source boundary conditions of their previously entangled state. In the present model, Bell correlations are computed from disentangled separated waves, boundary conditions of nonlinear optics, and properties of single-photon and vacuum states specified by quantum electrodynamics. Transient interference is assumed between photon-excited waves and photon-empty waves based on the possibility of such interference found to be necessary by the designers of Bell-experiment sources. The present model employs local random variables without specifying underlying causality.

Keywords

Bell Correlation, Bell Theorem, Locality, Wave-Particle Duality, Entanglement, Photon State

1. Introduction

The Bell theorem and violation of Bell's inequalities by experimentally acquired data sets have been believed to make the derivation of Bell correlations impossible without the existence of a perpetual entanglement based non-locality. However, it is shown in [1] that the mere existence of three or four data sets of ±1's, whether their origin is in experimental observation or counterfactual prediction, implies cross-correlations that identically satisfy the corresponding Bell inequa-

lity independently of Bell's assumptions, and even of whether the data are random. The cross-correlations among data sets may have varying functional forms, except for special processes such as wide sense stationarity. In the quantum mechanical case, conditional probabilities due to non-commutation of measurements beyond one per particle produce sets of correlations that are different from those assumed by Bell. The claim that experimental data violate the Bell inequality is commonly based on the use of six or eight data sets obtained in statistically independent pairs instead of the three or four cross-correlated sets used in the original derivation of the corresponding Bell inequality. Unsurprising, the inequality is violated. (See [1] for a detailed discussion of the issues summarized above).

As stated, Bell's assumptions in deriving the Bell inequality are unnecessary: it holds under general mathematical conditions without them. Of course, nullifying the Bell theorem does not automatically imply that a local model for the Bell correlation in the absence of entanglement is possible. However, superimposed wave pairs originating in spontaneous-parametric-down-conversion (SPDC) crystals become physically separated by experimental design, implying that Bell correlations can occur among photons attached to un-entangled local wave pairs due to physical source boundary conditions.

The current paper provides a calculation of the Bell correlation that begins with the principle that physically separated, non-superimposed, electromagnetic waves do not instantaneously influence each other. (The notion that they do is based on the flawed interpretation of Bell experiments stated above.) The correlations are computed from waves originating in nonlinear interactions, and standard interpretations of quantum electro-dynamic (QED) photon-wave properties. The originally entangled waves, some containing photons, others photon empty, later transiently interfere, consistent with the design [2] [3] of Bell-experiment sources. Further assumptions used in the model are that light consists of photons and waves, and that single photons do not divide at beam splitters, although interference still occurs at interferometer outputs (see Jacque, *et al.* [4]).

In QED theory, the quantum states of electromagnetic waves consist of ground/vacuum states and excited states that are interpreted as photons. The excited states are thus assumed herein to consist of photons attached to waves while the ground state is interpreted as a photon-empty wave. A recent classic experiment by Jacque, *et al.* [4] suggests that photon and associated vacuum states may interfere, and that interpretation is adopted in the present model. It is also consistent with the stated design of Bell experiments, for which it was found necessary to enable interference between photon wave states and vacuum wave states by equalizing optical paths. Thus modern experiments suggest that light is a composite of waves and attached photons rather than an entity that switches from particle-like to wave-like behavior depending on experimental circumstances.

However, the fact that little is actually known about photons complicates ef-

forts to develop a local physical model for the Bell correlation dependent on initial conditions at photon creation. In addition, properties of the quantum vacuum state are not well known, as its magnitude as given by QED has been called into serious question. (See Meis [5] for enumeration of various quantitative discrepancies and their discussion). Thus, in the following, use of the QED values for photon-containing and photon-empty waves is to be viewed as a specific hypothesis that leads to a derivation of the Bell correlation.

Two pairs of orthogonally polarized waves (see **Figure 1**), one photon attached to each pair, are emitted by an SPDC source with an added path equalization component (see source design in [2] [3]). Interference between polarization components of a photon-containing wave and an accompanying photon-empty wave occurs in coordinate systems rotated with respect to the original SPDC source system of coordinates. The phases of waves are assumed to be statistically independent of their amplitudes as is also consistent with the phase uncertainty of single photon states. Phase matching conditions of SPDC together with energy conservation constrain phase sums, but allow phase differences that may fluctuate over successive photon and vacuum waves. No mechanism is specified for the association of photons with waves beyond the formalism of QED [6], nonlinear optics, and experimental observation. Interactions are assumed to be local but variables' local behavior is random without attempts at further hidden variable explanations rooted in detailed photonic behavior.

The formalism of this paper begins in a way that is parallel to that used in [7]. However, the physical and probability models evolve differently. Local wave properties of light as employed here have also been used in [8] to account for polarization correlations of entangled photons after assuming circular polarization emanating from the source.

2. Bell Correlations from Local Pairs of Photons

Based on the geometry of type II SPDC sources for Bell correlation experiments

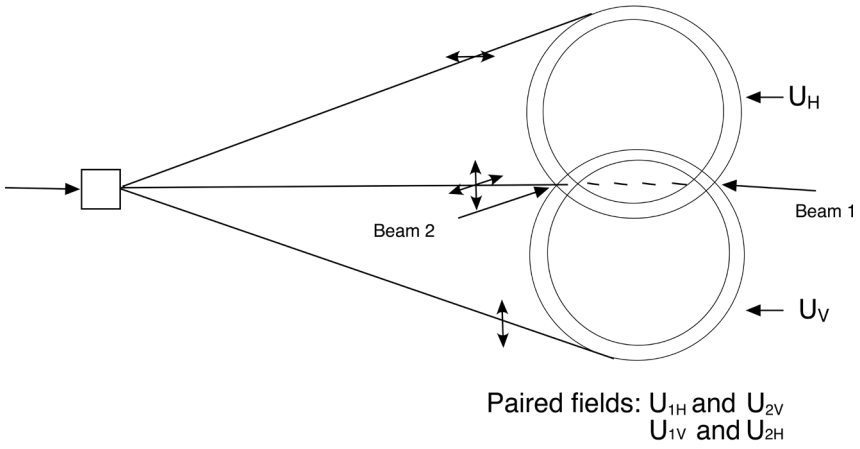

Figure 1. Output light cones of an SPDC in type II configuration (see [3]). In experiments, two apertures at the intersections of the light cones indicated result in formation of unpolarized beams 1 and 2 used in Bell experiments.

[2] [3], two amplitudes $\boldsymbol{U}_1$ and $\boldsymbol{U}_2$ are introduced representing Beams 1 and 2 of the Figure. These are vector amplitudes that result from super-positions of orthogonal vector components $u_{iH}, u_{iV}, i = 1, 2$. Thus,

$$\boldsymbol{U}_1 = u_{1H}\hat{i} + u_{1V}\hat{j} \tag{2.1a}$$

and

$$\boldsymbol{U}_2 = u_{2H}\hat{i} + u_{2V}\hat{j}. \tag{2.1b}$$

Initial horizontal and vertical amplitudes are indicated by subscripts H and V that correspond to unit vectors $\hat{i}$ and $\hat{j}$ respectively. The H and V components are both present in two secondary source regions labeled Beam 1 and Beam 2 in the figure as used in Bell experiments. (For simplicity, finite beam effects such as diffraction are neglected in the following model).

The components are given more explicitly as:

$$\begin{aligned} u_{1H} &= |u_{1H}|\cos\left(\theta_{1H} + \omega_{1H}t + 2\pi x/\lambda_{1H}\right); \\ u_{1V} &= |u_{1V}|\cos\left(\theta_{1V} + \omega_{1V}t + 2\pi x/\lambda_{1V}\right); \\ u_{2H} &= |u_{2H}|\cos\left(\theta_{2H} + \omega_{2H}t + 2\pi x/\lambda_{2H}\right); \\ u_{2V} &= |u_{2V}|\cos\left(\theta_{2V} + \omega_{2V}t + 2\pi x/\lambda_{2V}\right), \end{aligned} \tag{2.2}$$

where subscript pairs 1H-2V and 1V-2H correspond to phase-matched conservation-of-energy linked wave pairs in the down-converter source. Coordinate x is measured from the output plane of the source to the four detectors, all assumed to be equidistant from the source.

The experimental requirements of nonlinear optics (phase matching and conservation of energy) are assumed so that pairs of photons are emitted at random, one photon per amplitude pair in each of Beams 1 and 2. Each beam thus has a photon containing amplitude component and an orthogonally polarized photon-empty component. From the requirements of SPDC type II, each emitted photon pair has either polarizations 1H-2V or 1V-2H, each occurring with probability one half, where the numerals indicate the beams into which the photons are deposited. The laser pump intensity is adjusted so that two such events, *i.e.* four photons, rarely occur simultaneously.

Four QED-ground-state waves to which two photons per emission event become attached are assumed to be initially present in the crystal. The SPDC crystals are configured to produce wave-pair components 1H2V and 1V2H that separate to become Beams 1 and 2, and propagate to individual polarization analyzer-detectors on sides A and B of Bell experiments. Equal optical paths between the source and the four detectors are assumed. In the source crystal, phase matching occurs for each wave pair due to the symmetry of the source crystal structure [2] [3]. A compensator crystal, rotated 90˚ with respect to the first, results in all the beams having traversed equal optical paths after exiting the assembly so that orthogonal component pairs in Beams 1 and 2 may exhibit transient interference in analyzer outputs.

Due to the experimental design used, the polarization beam splitters on sides

A and B of a Bell experiment will be illuminated by beams having random polarizations. The polarization components in the transmit-reflect directions will be linear combinations of the components of the orthogonal pairs in Beams 1 and 2 indicated above.

The action of polarization analyzers placed in each of Beams 1 and 2 is now computed. Transmit and reflect components of $\boldsymbol{U}_1$ and $\boldsymbol{U}_2$ depend on the angle of rotation of the analyzer with respect to the $\hat{i}$ direction. Orthogonal unit vectors in the (n) and (p) directions of the two analyzers are

$$\hat{n}_{ln} = \cos\theta_l \hat{i} + \sin\theta_l \hat{j}, \ \hat{n}_{lp} = -\sin\theta_l \hat{i} + \cos\theta_l \hat{j}, \ \ l = 1,2 \tag{2.3}$$

From these, one obtains the analyzer's transmitted and reflected output amplitudes based on inputs (2.1) and (2.2):

$$\begin{aligned} U_{ln} &\equiv \boldsymbol{U}_l \cdot \hat{n}_{ln} = u_{lH}\cos\theta_l + u_{lV}\sin\theta_l, \\ U_{lp} &\equiv \boldsymbol{U}_l \cdot \hat{n}_{lp} = -u_{lH}\sin\theta_l + u_{lV}\cos\theta_l. \end{aligned} \quad l = 1,2 \tag{2.4a}$$

The instantaneous intensities of the analyzer output components n and p for each of the inputs $\boldsymbol{U}_1$ and $\boldsymbol{U}_2$ are given by

$$I_{ln} = U_{ln}^2; \ I_{lp} = U_{lp}^2, \ l = 1,2 \tag{2.4b}$$

where I_{1n} is explicitly evaluated using (2.2) to clarify the notation:

$$\begin{aligned} I_{1n} &= |u_{1H}|^2 \cos^2(\theta_{1H} + \omega_{1H}t + 2\pi x/\lambda_{1H})\cos^2\theta_1 \\ &\quad + |u_{1V}|^2 \cos^2(\theta_{1V} + \omega_{1V}t + 2\pi x/\lambda_{1V})\sin^2\theta_1 \\ &\quad + |u_{1H}||u_{1V}|\cos(\theta_{1H} + \omega_{1H}t + 2\pi x/\lambda_{1H})\cos(\theta_{1V} + \omega_{1V}t + 2\pi x/\lambda_{1V})\sin 2\theta_1. \end{aligned} \tag{2.5}$$

This can be simplified by performing short time averages over terms that oscillate at optical frequency: $\cos(\theta + \omega t)$. These fast oscillations play no role in the model calculation. Thus Equation (2.5) becomes:

$$\begin{aligned} I_{1n} &= \frac{|u_{1H}|^2 \cos^2\theta_1}{2} + \frac{|u_{1V}|^2 \sin^2\theta_1}{2} \\ &\quad + \frac{|u_{1H}||u_{1V}|\cos\left[(\theta_{1H} - \theta_{1V}) + (\omega_{1H} - \omega_{1V})t + 2\pi x(1/\lambda_{1H} - 1/\lambda_{1V})\right]\sin 2\theta_1}{2} \\ &= I_{1H}\cos^2\theta_1 + I_{1V}\sin^2\theta_1 \\ &\quad + \sqrt{I_{1H}I_{1V}}\cos\left[(\theta_{1H} - \theta_{1V}) + (\omega_{1H} - \omega_{1V})t + 2\pi x(1/\lambda_{1H} - 1/\lambda_{1V})\right]\sin 2\theta_1 \end{aligned} \tag{2.6}$$

where absolute-value-squared amplitudes divided by 2 are replaced by equivalent average intensities and the only retained term dependent on time occurs at a lower beat frequency. In a similar manner

$$\begin{aligned} I_{1p} &= I_{1H}\sin^2\theta_1 + I_{1V}\cos^2\theta_1 \\ &\quad - \sqrt{I_{1H}I_{1V}}\cos\left[(\theta_{1H} - \theta_{1V}) + (\omega_{1H} - \omega_{1V})t + 2\pi x(1/\lambda_{1H} - 1/\lambda_{1V})\right]\sin 2\theta_1. \end{aligned} \tag{2.7}$$

The original source intensities at $\theta_1 = 0$ are then $I_{1n}(0) = I_{1H}$ and $I_{1p}(0) = I_{1V}$. For analyzer 2 one obtains

$$\begin{aligned} I_{2n} &= I_{2H}\cos^2\theta_2 + I_{2V}\sin^2\theta_2 \\ &\quad + \sqrt{I_{2H}I_{2V}}\cos\left[(\theta_{2H} - \theta_{2V}) + (\omega_{2H} - \omega_{2V})t + 2\pi x(1/\lambda_{2H} - 1/\lambda_{2V})\right]\sin 2\theta_2 \end{aligned} \tag{2.8}$$

and

$$I_{2p} = I_{2H}\sin^2\theta_2 + I_{2V}\cos^2\theta_2 - \sqrt{I_{2H}I_{2V}}\cos\left[\left(\theta_{2H}-\theta_{2V}\right)+\left(\omega_{2H}-\omega_{2V}\right)t+2\pi x\left(1/\lambda_{2H}-1/\lambda_{2V}\right)\right]\sin 2\theta_2. \quad (2.9)$$

At $\theta_2 = 0, I_{2n}(0) = I_{2H}$ and $I_{2p}(0) = I_{2V}$.

The equations may be simplified by using specifications of nonlinear optics [9] in SPDC-phase matching and symmetry of the source:

$$\theta_{2H} + \theta_{1V} = const + \Delta_{2H}, \quad \theta_{2V} + \theta_{1H} = const + \Delta_{2V}, \quad (2.10a)$$

where the Δ's are additional phase shifts implemented by a wave plate used in experiments [2] [3]. The difference of phases in the two beams is then

$$\theta_{2H} - \theta_{2V} = \theta_{1H} - \theta_{1V} + \Delta_{2H} - \Delta_{2V}. \quad (2.10b)$$

The condition $\Delta_{2H} - \Delta_{2V} = \pi$, is experimentally implemented so that

$$\theta_{2H} - \theta_{2V} = \theta_{1H} - \theta_{1V} + \pi \quad (2.10c)$$

In addition, angular oscillation frequencies of (2.6-2.9) are related through conservation of energy relations in the nonlinear source:

$$\omega_{1H} + \omega_{2V} = \omega_p; \quad \omega_{1V} + \omega_{2H} = \omega_p \quad (2.10d)$$

where ω_p equals the angular frequency of the pump from which the pairs of photons are derived in the nonlinear process. From the relations of Equation (2.10d) it follows that

$$\omega_{1H} - \omega_{1V} = \omega_{2H} - \omega_{2V}: \quad 1/\lambda_{1H} - 1/\lambda_{1V} = 1/\lambda_{2H} - 1/\lambda_{2V}, \quad (2.10e)$$

where the maximum relative frequency variation between the beams has been estimated as [3] $d\omega/\omega = 0.007$. While conditions (2.10a-e) are physically reasonable, a separate experimental study of source properties would be necessary to confirm them in detail.

When (2.10c) and (2.10e) are used in (2.6-2.9), one obtains

$$I_{1n} = I_{1H}\cos^2\theta_1 + I_{1V}\sin^2\theta_1 + \sqrt{I_{1H}I_{1V}}\cos\left[\left(\theta_{1H}-\theta_{1V}\right)+\left(\omega_{1H}-\omega_{1V}\right)t+2\pi x\left(1/\lambda_{1H}-1/\lambda_{1V}\right)\right]\sin 2\theta_1$$

$$I_{1p} = I_{1H}\sin^2\theta_1 + I_{1V}\cos^2\theta_1 - \sqrt{I_{1H}I_{1V}}\cos\left[\left(\theta_{1H}-\theta_{1V}\right)+\left(\omega_{1H}-\omega_{1V}\right)t+2\pi x\left(1/\lambda_{1H}-1/\lambda_{1V}\right)\right]\sin 2\theta_1$$

$$I_{2n} = I_{2H}\cos^2\theta_2 + I_{2V}\sin^2\theta_2 - \sqrt{I_{2V}I_{2H}}\cos\left[\left(\theta_{1H}-\theta_{1V}\right)+\left(\omega_{1H}-\omega_{1V}\right)t+2\pi x\left(1/\lambda_{1H}-1/\lambda_{1V}\right)\right]\sin 2\theta_2$$

$$I_{2p} = I_{2H}\sin^2\theta_2 + I_{2V}\cos^2\theta_2 + \sqrt{I_{2V}I_{2H}}\cos\left[\left(\theta_{1H}-\theta_{1V}\right)+\left(\omega_{1H}-\omega_{1V}\right)t+2\pi x\left(1/\lambda_{1H}-1/\lambda_{1V}\right)\right]\sin 2\theta_2 \quad (2.11a\text{-}d)$$

Since the phase differences are not determined by Equations (2.10a-c, e), the value of $\cos\left[\left(\theta_{1H}-\theta_{1V}\right)+\left(\omega_{1H}-\omega_{1V}\right)t+2\pi x\left(1/\lambda_{1H}-1/\lambda_{1V}\right)\right]$ varies randomly over the interval +1 to −1 depending on the precise phases, frequency, wavelength of the light, and photon pulse occurrence time, and averages to zero over random photon occurrence times, while

$\cos^2\left[\left(\theta_{1H}-\theta_{1V}\right)+\left(\omega_{1H}-\omega_{1V}\right)t+2\pi x\left(1/\lambda_{1H}-1/\lambda_{1V}\right)\right]$ averages to 1/2. The relative phases among the waves as they exit the source are maintained at equal times/distances from the source since they all propagate with the same velocity. Note however, that if $\omega_{1H}=\omega_{1V}$ and $\lambda_{1H}=\lambda_{1V}$, i.e., the original entangled waves have the same wavelength and frequency, that the detectors can be at different distances from the source without affecting the results to be derived below.

For the physical situation considered, the two equations of (2.10a) correspond alternately to photon-containing wave pairs and vacuum wave pairs. It is not clear whether phase behavior differences should be attributed to waves depending on whether they do or do not contain photons. However, to obtain agreement with correlations that result from physical entanglement and enable wave interference, the phase conditions that hold for photon-containing waves will be assumed to hold for photon-empty waves.

The individual intensity variables (2.11a-d) are now interpreted from QED to clarify their later use in computation of the Bell correlation. The use of QED concepts will be illustrated for variables I_{1n} and I_{1p} where these wave-pulse intensities will be defined as proportional to the QED photon energies when counts occur. Computations will be carried out for two alternative sets of relative intensities based on the QED [6] description of a single photon state:

$I_{1H}=I_{2V}=1$ for a photon wave-pulse, $I_{1V}=I_{2H}=1/2$ for vacuum waves,

or

$I_{1V}=I_{2H}=1$ for a photon wave-pulse, $I_{1H}=I_{2V}=1/2$ for vacuum waves,

each condition occurring with probability 1/2 over photon-pair emission events, and with energies/intensities given in units of $h\nu$ by QED for photon pulses in observation time windows. Angle $\left[\theta_{1H}-\theta_{1V}+\left(w_{1H}-\omega_{1V}\right)t+2\pi x\left(1/\lambda_{1N}-1/\lambda_{1V}\right)\right]$ is replaced by θ, and as stated above, $\overline{\cos\theta}=0$ over randomly occurring beats evaluated at photon occurrence times.

Since beam intensities are measured by photon occurrences, the intensities for photon pair production events 1H2V and 1V2H are equal: $I_{1H}=I_{2V}$ and $I_{1V}=I_{2H}$ if the less than 1% frequency variation among the relevant beams is neglected. Beam intensity pairs without photon occurrences are assumed to be equal also, and in accordance with QED to have intensity 1/2. The corresponding beam amplitudes are given by the square roots of the intensities. (Overbars and rectangular brackets are used interchangeably to denote averages below).

The mean of I_{1n} in Equation (2.11a) under the above source specification is given by

$$\begin{aligned}\overline{I_{1n}}=&\frac{1}{2}\left(1\cos^2\theta_1+(1/2)\sin^2\theta_1+1\cdot\left(1/\sqrt{2}\right)\overline{\cos\theta}\sin 2\theta_1\right)_{1H}\\&+\frac{1}{2}\left((1/2)\cos^2\theta_1+1\sin^2\theta_1+1\cdot\left(1/\sqrt{2}\right)\overline{\cos\theta}\sin 2\theta_1\right)_{1V}\end{aligned}\tag{2.12a}$$

where subscripts on the parentheses indicate which input variable is associated with a photon. Similarly, the mean of I_{1p} from Equation (2.11b) is

$$\begin{aligned}\overline{I_{1p}} &= \frac{1}{2}\left(1\sin^2\theta_1 + (1/2)\cos^2\theta_1 - 1\cdot\left(1/\sqrt{2}\right)\overline{\cos\theta}\sin 2\theta_1\right)_{1H} \\ &+ \frac{1}{2}\left((1/2)\sin^2\theta_1 + 1\cos^2\theta_1 - 1\cdot\left(1/\sqrt{2}\right)\overline{\cos\theta}\sin 2\theta_1\right)_{1V}\end{aligned} \tag{2.12b}$$

Equations (2.12a, b) become

$$\overline{I_{1n}} = \frac{1}{2}\left(1\cos^2\theta_1\right)_{1H} + \frac{1}{2}\left(1\sin^2\theta_1\right)_{1V} = \frac{1}{2} \tag{2.12c}$$

and

$$\overline{I_{1p}} = \frac{1}{2}\left(1\sin^2\theta_1\right)_{1H} + \frac{1}{2}\left(1\cos^2\theta_1\right)_{1V} = \frac{1}{2}, \tag{2.12d}$$

after deleting terms with coefficient 1/2, and setting $\overline{\cos\theta}$ equal to 0 over averaged photon events and times. Terms with coefficient 1/2 correspond to pure vacuum contributions to intensities I_{1n} and I_{1p} and are invisible to detectors. They also have different frequencies from the photon-carrying waves. The $\cos\theta$ term alternately increases and decreases probabilities of I_{1n} and I_{1p}, but averages to zero over multiple photon counts.

The correlation of I_{1n} and I_{1p} is now computed for photon occurrences 1H and 1V, that occur with probability 1/2, respectively

$$\begin{aligned}\left\langle I_{1n}I_{1p}\right\rangle_{1H} &= \left\langle\left(1\cos^2\theta_1 + (1/2)\sin^2\theta_1 + 1\cdot\left(1/\sqrt{2}\right)\cos\theta\sin 2\theta_1\right)_{1H}\right. \\ &\left.\times\left(1\sin^2\theta_1 + (1/2)\cos^2\theta_1 - 1\cdot\left(1/\sqrt{2}\right)\cos\theta\sin 2\theta_1\right)_{1H}\right\rangle \\ &= 1\cdot 1\cos^2\theta_1\sin^2\theta_1 + 1\cdot(1/2)\cos^4\theta_1 + (1/2)\cdot 1\sin^4\theta_1 \\ &+ (1/2)^2\sin^2\theta_1\cos^2\theta_1 - (1/2)\overline{\cos^2\theta}\sin^2 2\theta_1 \\ &= 1\cdot 1\cos^2\theta_1\sin^2\theta_1 - (1/2)^2\sin^2 2\theta_1 = 0,\end{aligned} \tag{2.13a}$$

where first power terms in $\overline{\cos\theta}$ have been averaged to zero over multiple events. Similarly

$$\begin{aligned}\left\langle I_{1n}I_{1p}\right\rangle_{1V} &= \left\langle\left((1/2)\cos^2\theta_1 + 1\sin^2\theta_1 + 1\cdot\left(1/\sqrt{2}\right)\cos\theta\sin 2\theta_1\right)_{1V}\right. \\ &\left.\times\left((1/2)\sin^2\theta_1 + 1\cos^2\theta_1 - 1\cdot\left(1/\sqrt{2}\right)\cos\theta\sin 2\theta_1\right)_{1V}\right\rangle \\ &= (1/4)\cos^2\theta_1\sin^2\theta_1 + 1\cdot(1/2)\cos^4\theta_1 + (1/2)\cdot 1\sin^4\theta_1 \\ &+ 1\cdot 1\sin^2\theta_1\cos^2\theta_1 - (1/2)\overline{\cos^2\theta}\sin^2 2\theta_1 \\ &= 1\cdot 1\sin^2\theta_1\cos^2\theta_1 - (1/2)^2\sin^2 2\theta_1 = 0.\end{aligned} \tag{2.13b}$$

The evaluation of Equations (2.13a, b) has been carried out so as to be consistent with the response of two separated detectors, each assumed to have an efficiency of 1 for detection of photons but to be blind to vacuum waves. As a result, terms having a coefficient consisting of a single or no 1's multiplied by factors of 1/2 are dropped since they correspond to the possibility of activation of only one detector or none. The term with two 1's in the coefficient, multiplied by the probabilities of detection by alternate detectors, is canceled by the interference

term. Thus,

$$\left\langle I_{1n}I_{1p}\right\rangle = \frac{1}{2}\left\langle I_{1n}I_{1p}\right\rangle_{1H} + \frac{1}{2}\left\langle I_{1n}I_{1p}\right\rangle_{1V} = 0, \tag{2.14}$$

consistent with the requirement that photons arrive at either detector 1n or 1p, resulting in a count correlation of zero. It should be noted that the interference terms in Equations (2.11a) and (2.11b) are of opposite sign, as are the resulting fluctuations of intensities I_{1n} and I_{1p} that ultimately specify the average count rates at detectors 1n and 1p. Since each detector then receives an average of half the photons created, the average of $I_{1n}+I_{1p}$ equals 1.

The assumption (indicated by experimental observation) that vacuum waves may interfere with photon bearing waves so as to affect the probability of photon detection yields reasonable results in the above calculations. It should be noted that the different interpretations of photon and non-photon terms follow from the experimental result that photons are not divided at beam splitters while wave intensities are divided. Thus for a photon containing wave, although sine and cosine squared terms correspond to wave division, they also indicate probabilities of photon deflection, but for a vacuum wave, they are interpreted as wave intensity division only.

The same interpretation of the photon pair production process used above may be used on the other equations of (2.11a-d). From the photon probability variables given in (2.11a-d), one may compute the joint intensity or photon count correlations in terms of products such as $I_{1n}I_{2p}$. As above, since $\left[\theta_{1H}-\theta_{1V}+\left(w_{1H}-\omega_{1V}\right)t+2\pi x\left(1/\lambda_{1H}-1/\lambda_{1V}\right)\right]$ is assumed to vary over 2π given random phases and times of photon occurrence, $\overline{\cos\theta}=0$, with its square equal to 1/2 in product terms. Starting from (2.11a, d), the multi-event correlation is

$$\begin{aligned}\left\langle I_{1n}I_{2p}\right\rangle = \Big\langle & I_{1H}I_{2H}\cos^2\theta_1\sin^2\theta_2 + I_{1V}I_{2V}\sin^2\theta_1\cos^2\theta_2 + I_{1H}I_{2V}\cos^2\theta_1\cos^2\theta_2 \\ & + I_{1V}I_{2H}\sin^2\theta_1\sin^2\theta_2 + \sqrt{I_{1H}I_{1V}}\sqrt{I_{2H}I_{2V}}\,\overline{\cos^2\theta}\sin 2\theta_1\sin 2\theta_2\Big\rangle,\end{aligned} \tag{2.15}$$

where averaging has already been applied to cross-terms involving $\cos\theta$ in (2.15).

Further evaluation of (2.15) will be shown in detail to illustrate the use of the SPDC generation of photon pairs under the QED model:
$I_{1H}=I_{2V}=1, I_{1V}=I_{2H}=1/2$ or $I_{1V}=I_{2H}=1, I_{1H}=I_{2V}=1/2$, each occurring with probability 1/2. Then

$$\begin{aligned}\left\langle I_{1n}I_{2p}\right\rangle = \frac{1}{2}\Bigg[& 1\cdot\frac{1}{2}\cos^2\theta_1\sin^2\theta_2 + \frac{1}{2}\cdot 1\sin^2\theta_1\cos^2\theta_2 + 1\cdot 1\cos^2\theta_1\cos^2\theta_2 \\ & + \frac{1}{2}\cdot\frac{1}{2}\sin^2\theta_1\sin^2\theta_2 + \sqrt{1\cdot\frac{1}{2}}\cdot\sqrt{\frac{1}{2}\cdot 1}\,\frac{1}{2}\sin 2\theta_1\sin 2\theta_2\Bigg]_{1H2V} \\ & + \frac{1}{2}\Bigg[\frac{1}{2}\cdot 1\cos^2\theta_1\sin^2\theta_2 + 1\cdot\frac{1}{2}\sin^2\theta_1\cos^2\theta_2 + \frac{1}{2}\cdot\frac{1}{2}\cos^2\theta_1\cos^2\theta_2 \\ & + 1\cdot 1\sin^2\theta_1\sin^2\theta_2 + \sqrt{\frac{1}{2}\cdot 1}\sqrt{1\cdot\frac{1}{2}}\,\frac{1}{2}\sin 2\theta_1\sin 2\theta_2\Bigg]_{1V2H}.\end{aligned} \tag{2.16}$$

The square brackets' subscripts indicate the alternative ways that two photons may occur, each with probability 1/2. The terms that imply the possibility of one photon being contributed to each of I_{1n} and I_{2p} are those having a product of two 1's in their coefficients. These terms are the third term in the first square bracket, the fourth term in the second bracket and the two interference terms involving square roots, one from each bracket. The contributions from these terms add to

$$\begin{aligned}\overline{I_{1n}I_{2p}} &= \frac{1}{2}\left[1\cdot 1\cos^2\theta_1\cos^2\theta_2 + 1\cdot 1\sin^2\theta_1\sin^2\theta_2 + 2\sin\theta_1\cos\theta_1\sin\theta_2\cos\theta_2\right] \\ &= \frac{1}{2}\cos^2(\theta_1-\theta_2).\end{aligned} \tag{2.17a}$$

From similar analysis, one computes the other correlations:

$$\overline{I_{1p}I_{2n}} = \frac{1}{2}\cos^2(\theta_1-\theta_2); \quad \overline{I_{1n}I_{2n}} = \overline{I_{1p}I_{2p}} = \frac{1}{2}\sin^2(\theta_1-\theta_2). \tag{2.17b}$$

By attaching minus signs to the 1p2n and 1n2p averages one obtains the same result as computed from entanglement,

$$-\overline{I_{1n}I_{2p}} - \overline{I_{1p}I_{2n}} + \overline{I_{1n}I_{2n}} + \overline{I_{1p}I_{2p}} = -\cos 2(\theta_1-\theta_2), \tag{2.18}$$

which is the Bell correlation.

It is useful to re-derive (2.18) in an alternate way to illustrate the internal consistency of the method. The definition of functions $S_1(\theta_1)$ and $S_2(\theta_2)$ is

$$\begin{aligned}S_1(\theta_1) &= I_{1n} - I_{1p} = (I_{1H} - I_{1V})\cos 2\theta_1 + 2\sqrt{I_{1H}I_{1V}}\cos\theta\sin 2\theta_1 \\ S_2(\theta_2) &= I_{2n} - I_{2p} = -(I_{2V} - I_{2H})\cos 2\theta_2 - 2\sqrt{I_{2V}I_{2H}}\cos\theta\sin 2\theta_2\end{aligned} \tag{2.19}$$

Computations are again carried out under alternative QED conditions $I_{1H} = I_{2V} = 1$, $I_{1V} = I_{2H} = 1/2$, and $I_{1V} = I_{2H} = 1$, $I_{1H} = I_{2V} = 1/2$, each with probability 1/2. Consistent with this, one obtains

$$\begin{aligned}\overline{S_1} = \langle I_{1n} - I_{1p}\rangle &= \frac{1}{2}\left(1\cos 2\theta_1 + 2\cdot 1\cdot\left(1/\sqrt{2}\right)\overline{\cos\theta}\sin 2\theta_1\right)_{1H} \\ &+ \frac{1}{2}\left(-1\cos 2\theta_1 + 2\cdot 1\cdot\left(1/\sqrt{2}\right)\overline{\cos\theta}\sin 2\theta_1\right)_{1V} = 0,\end{aligned} \tag{2.20}$$

since $\overline{\cos\theta} = 0$. Similarly, $\overline{S_2(\theta_2)} = 0$ and $\overline{S_1^2} = \overline{S_2^2} = 1$. One may now calculate the Bell correlation as a multi-event average and replace first power terms involving $\overline{\cos\theta}$ with zeros:

$$\begin{aligned}\overline{S_1(\theta_1)S_2(\theta_2)} &= \Big\langle -(I_{1H} - I_{1V})(I_{2V} - I_{2H})\cos 2\theta_1\cos 2\theta_3 \\ &\quad - 4\sqrt{I_{1H}I_{1V}I_{2V}I_{2H}}\,\overline{\cos^2\theta}\sin 2\theta_1\sin 2\theta_2\Big\rangle \\ &= \frac{1}{2}\left[(-1)(1)\cos 2\theta_1\cos 2\theta_2 - 4\frac{1}{2}\frac{1}{2}\sin 2\theta_1\sin 2\theta_2\right]_{1H\,2V} \\ &\quad + \frac{1}{2}\left[(1)(-1)\cos 2\theta_1\cos 2\theta_2 - 4\frac{1}{2}\frac{1}{2}\sin 2\theta_1\sin 2\theta_2\right]_{1V\,2H} \\ &= -\cos 2(\theta_1-\theta_2).\end{aligned} \tag{2.21}$$

Thus, the methodology used to compute the Bell correlation gives consistent

results under the assumptions used to derive it: factors corresponding to photon pairs have intensities 1 as specified by QED while interfering vacuum waves have intensities 1/2. The vacuum waves do not contribute to observed counts except as they interfere with waves corresponding to counts.

3. Conclusions

A number of authors have found reason to question the Bell theorem [10]. The theorem is purported to be a proof that no local hidden variable model of the Bell correlation can be constructed. The fact that the Bell inequality must be identically satisfied by any data sets measured experimentally or from counterfactual prediction, invalidates the theorem since it follows that quantum mechanical data, once obtained and cross-correlated cannot violate the inequality. Nevertheless, invalidation of the theorem does not in itself imply that local physical models not explicitly computed from entanglement exist for the correlations.

The present work develops a version of a local probability model for the Bell correlation using explicitly separated un-entangled waves, boundary conditions based on nonlinear optics, QED, and transient interference between quantum vacuum-state waves and waves with attached photons. The model is idealized, but that is consistent with our level of understanding of photons and vacuum waves. The Bell correlation results from averaging over many particle pair events but necessarily differs in some details from the conventional model based on entanglement that assumes two spatially separated measurements performed on a perpetual superposition of four waves. Such a perpetual superposition is inconsistent with electro-magnetic wave propagation as known outside of the fatally flawed Bell theorem.

Acknowledgements

The author would like to thank Michael Hall for a detailed critique of a previous version of this paper that aided in the current revision. He would also like to thank Joe Foreman for stimulating conversations prompting reconsideration of some issues.

Conflicts of Interest

The author declares no conflicts of interest regarding the publication of this paper.

References

[1] Sica, L. (2020) *Journal of Modern Physics*, **11**, 725-740. https://doi.org/10.4236/jmp.2020.115047

[2] Shih, Y. (2003) *Reports on Progress in Physics*, **66**, 1009-1044. https://doi.org/10.1088/0034-4885/66/6/203

[3] Kwiat, P.G., Mattle, K., Weinfurter, H., Zeilinger, A., Sergienko, A.V. and Shih, Y. (1995) *Physical Review Letters*, **75**, 4337-4342.

https://doi.org/10.1103/PhysRevLett.75.4337

[4] Jacques, V., Wu, E., Grosshans, F., Treussart, F., Grangier, P., Aspect, A. and Roch, J.F. (2007) *Science*, **315**, 966-968. https://doi.org/10.1126/science.1136303

[5] Meis, C. (2017) Light ad Vacuum. 2nd Edition, World Scientific, Hackensack, New Jersey.

[6] Loudon, R. (2000) The Quantum Theory of Light. 3rd Edition, Oxford University Press Inc., New York, Chap. 4.

[7] Sica, L. (2014) *Applied Mathematics*, **5**, 2899-2907. https://doi.org/10.4236/am.2014.518276

[8] Jung, K. (2020) *Frontiers in Physics*, **8**, 170. https://doi.org/10.3389/fphy.2020.00170

[9] Smith, R.G. (1970) *Journal of Applied Physics*, **41**, 4121-4124. https://doi.org/10.1063/1.1658422

[10] Hess, K., De Raedt, H. and Khrennikov, A. (2017) *Open Physics*, **15**, 572-576. https://doi.org/10.1515/phys-2017-0067

Journal of Modern Physics, 2021, 12, 22-34
https://www.scirp.org/journal/jmp
ISSN Online: 2153-120X
ISSN Print: 2153-1196

Stochastic Simulation of Emission Spectra and Classical Photon Statistics of Quantum Dot Superluminescent Diodes

Kai Niklas Hansmann, Reinhold Walser

Technische Universität Darmstadt, Institut für Angewandte Physik, Hochschulstraße 4a, Darmstadt, Germany
Email: kai.hansmann@physik.tu-darmstadt.de

How to cite this paper: Hansmann, K.N. and Walser, R. (2021) Stochastic Simulation of Emission Spectra and Classical Photon Statistics of Quantum Dot Superluminescent Diodes. *Journal of Modern Physics*, **12**, 22-34.
https://doi.org/10.4236/jmp.2021.121003

Received: November 27, 2020
Accepted: January 5, 2021
Published: January 8, 2021

Abstract

We present a stochastic procedure to investigate the correlation spectra of quantum dot superluminescent diodes. The classical electric field of a diode is formed by a polychromatic superposition of many independent stochastic oscillators. Assuming fields with individual carrier frequencies, Lorentzian linewidths and amplitudes we can form any relevant experimental spectrum using a least square fit. This is illustrated for Gaussian and Lorentzian spectra, Voigt profiles and box shapes. Eventually, the procedure is applied to an experimental spectrum of a quantum dot superluminescent diode which determines the first- and second-order temporal correlation functions of the emission. We find good agreement with the experimental data and a quantized treatment. Thus, a superposition of independent stochastic oscillators represents the first- and second-order correlation properties of broadband light emitted by quantum dot superluminescent diodes.

Keywords

Stochastic Simulation, Quantum Dot, Superluminescent Diode

1. Introduction

Modern-day optical applications like optical coherence tomography [1] [2] and ghost imaging [3] [4] [5] make use of the unique emission properties of spectrally broadband light-emitting quantum dot superluminescent diodes (QDSLD). By using specialized waveguide geometries and gain materials, QDSLDs are able to combine high output intensities, spatially directed emission and spectral widths in the THz regime. Hence, they fill the gap in the family of semiconductor-based optical emitters between coherent laser diodes and incoherent light emitting

diodes. After being proposed in 1973 [6], research on the characteristics of QDSLDs has been intensified in recent years after Boitier *et al.* [7] enabled the direct measurement of coherence times in the femtosecond regime using two-photon absorption in semiconductors. This research is both theoretical and experimental nature. From the theoretical side, the understanding of light generation processes inside the diode is a main focus. For this, a plethora of approaches is being utilized including rate equation models [8] [9] [10], travelling wave approaches [11], finite element methods [12] and quantized treatments [13] [14]. Experimental studies focus on the determination of first- and second-order temporal correlation properties of QDSLDs [15] [16]. In 2011, *Blazek et al.* were able to observe a temperature dependent suppression of intensity fluctuations $g^{(2)}(\tau=0)<2$ using a broadband emitting QDSLD [17]. To this day, effort is being put into developing more efficient and high-powered QDSLDs [18] [19] [20].

Adding a new perspective to the investigation of QDSLDs, we discuss a stochastic model for the emission in this article. Stochastic approaches have long proven to have a wide-ranging field of applications in biology [21] [22] [23], engineering [24], finance [25], quantum many-body physics [26] [27], soft-matter physics [28] [29], optics [30] [31] and many more scientific areas. We develop a model to describe experimental emission spectra from a superposition of stochastic fields. Using least square fits, we determine Lorentzian linewidths, carrier frequencies and amplitudes of the individual fields to model experimental spectra. This is illustrated for Gaussian-, Lorentzian-, Voigt- as well as bandpass spectra and applied to the experimental spectrum of a QDSLD [3]. Using numerical simulations, we determine first- and second-order temporal correlation functions of the electric field and calculate the spectral power density of the resulting emission.

The article is organized as follows: the stochastic model of emission spectra is developed in Section 2. It consists of individual classical fields, which are described by a distinct stochastic differential equation. After investigating properties of these fields, relevant spectra are modelled as a superposition. This is applied to a specific experimental spectrum produced by a QDSLD [3]. The model is subsequently used to calculate the emission spectrum of the diode in Section 3 and the normalized stationary second-order temporal correlation function in Section 4. A conclusion is given in Section 5. An **Appendix** summarizes the convergence properties of the simulation schemes.

2. Stochastic Model of Emission Spectra

The classical electric field of a diode results from a superposition of stochastic fields. Hence, the electric field outside of the diode reads

$$\varepsilon_{\mathrm{d}}(t)=\sum_{j=1}^{N}\varepsilon_{j}(t), \tag{1}$$

with the number of fields N and $\varepsilon_j(t)$ the j-th complex field amplitude.

2.1. Ornstein-Uhlenbeck Process

An individual classical field $\varepsilon(t) \in \mathbb{C}$ is modelled as a complex Ornstein-Uhlenbeck process [32]. This is described by the Ito stochastic differential equation [33]

$$\mathrm{d}\varepsilon(t) = (\mathrm{i}\nu_0 - \gamma)\varepsilon(t)\mathrm{d}t + D\mathrm{d}W(t), \tag{2}$$

with the carrier frequency ν_0, the linewidth γ, the diffusion constant $D = \sqrt{\gamma I}$, the mean intensity of the electric field $I = \lim_{t\to\infty}\left\langle|\varepsilon(t)|^2\right\rangle$ and the complex Wiener noise increment $\mathrm{d}W(t) \in \mathbb{C}$, whose properties are given by $\left\langle \mathrm{d}W(t)\right\rangle = 0$ and $\left\langle|\mathrm{d}W(t)|^2\right\rangle = \mathrm{d}t$.

The stationary first-order temporal correlation function reads [33] [34]

$$G_{\mathrm{s}}^{(1)}(\tau) = \lim_{t\to\infty}\left\langle \varepsilon^*(t)\varepsilon(t+\tau)\right\rangle = I\mathrm{e}^{-\gamma|\tau|-\mathrm{i}\nu_0\tau}. \tag{3}$$

The spectral power density is given by the Fourier transform

$$S(\nu) = \frac{1}{\sqrt{2\pi}}\int_{-\infty}^{\infty}\mathrm{d}\tau\, G_{\mathrm{s}}^{(1)}(\tau)\mathrm{e}^{\mathrm{i}\nu\tau} \tag{4}$$

of (3) in accordance to the Wiener-Khintchine theorem [35] [36]. This yields

$$S(\nu) = I\sqrt{\frac{2}{\pi}}\frac{\gamma}{(\nu-\nu_0)^2+\gamma^2}, \quad \frac{1}{\sqrt{2\pi}}\int_{-\infty}^{\infty}\mathrm{d}\nu\, S(\nu) = I. \tag{5}$$

Furthermore, the stationary normalized second-order temporal correlation function is given by the Siegert relation [34] [37]

$$g_{\mathrm{s}}^{(2)}(\tau) = \lim_{t\to\infty}\frac{\left\langle \varepsilon^*(t)\varepsilon^*(t+\tau)\varepsilon(t+\tau)\varepsilon(t)\right\rangle}{\left\langle \varepsilon^*(t)\varepsilon(t)\right\rangle\left\langle \varepsilon^*(t+\tau)\varepsilon(t+\tau)\right\rangle} = 1+\mathrm{e}^{-2\gamma|\tau|}. \tag{6}$$

2.2. Stochastic Simulation

In addition to analytical results, we perform numerical simulations of (2). In order to obtain an efficient simulation procedure, we separate the rapid oscillating carrier frequency by the transformation $\varepsilon(t) = \eta(t)\mathrm{e}^{-\mathrm{i}\nu_0 t}$ yielding

$$\mathrm{d}\eta(t) = -\gamma\eta(t)\mathrm{d}t + D\mathrm{d}W(t). \tag{7}$$

As the diffusion constant D is independent of the electric field amplitude $\eta(t)$, the Euler scheme [38] can be used to achieve strong convergence of order 1.0 (see **Appendix**). Therefore the electric field amplitude can be simulated iteratively

$$\eta(t_{i+1}) = \eta(t_i) - \gamma\eta(t_i)\Delta t + D\Delta W, \tag{8}$$

with the discrete time step $\Delta t = t_{i+1} - t_i$ and ΔW a complex Gaussian random process with mean $\langle\Delta W\rangle = 0$ and variance $\left\langle|\Delta W|^2\right\rangle = \Delta t$.

The first-order temporal correlation function of (3) is calculated from a sample average over M realizations

$$G^{(1)}(\tau) = \frac{1}{M}\sum_{m=1}^{M}\left(\varepsilon^{(m)}(t_s)\right)^*\varepsilon^{(m)}(t_s+\tau) \tag{9}$$

long after the transient regime $t_s \gg 1/\gamma_j$. $\varepsilon^{(m)}(t)$ is the m-th realization of the

electric field. This result can be used to calculate the spectral power density of the emission using a Fourier transformation.

The determination of the normalized second-order temporal correlation function (6) can be split into two separate calculations. The first-order temporal correlation functions in the denominator can be simulated according to (9), while the second-order correlation function in the numerator can be calculated as

$$G^{(2)}(\tau)=\frac{1}{M}\sum_{m=1}^{M}\left|\varepsilon^{(m)}(t_s+\tau)\varepsilon^{(m)}(t_s)\right|^2. \tag{10}$$

Simulation results as well as analytical calculations of the first- and second-order temporal correlation properties of an individual field can be seen in Figure 1.

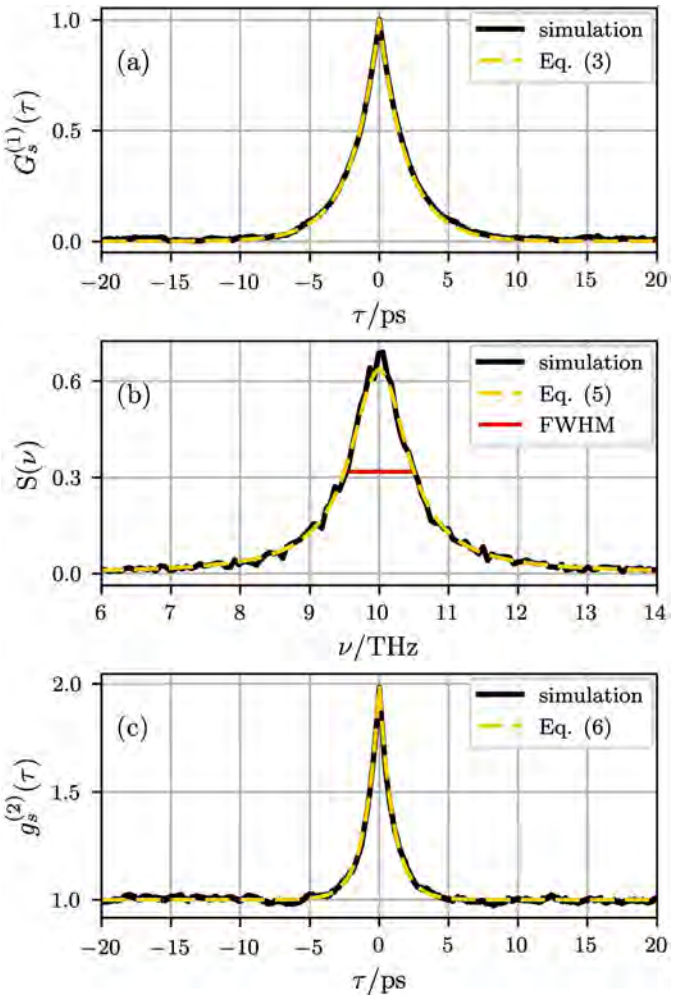

Figure 1. (a) Stationary first-order temporal correlation function $G_s^{(1)}(\tau)$ versus time τ, (b) spectral power density $S(\nu)$ versus frequency ν with width (FWHM) $2\gamma=1$ THz and (c) stationary normalized second-order temporal correlation function $g_s^{(2)}(\tau)$ versus time τ for the electric field described by (2). Simulation results (black, solid) and analytical expressions (yellow, dashed) were calculated with $I=1$ and $\nu_0=10$ THz. The correlation functions were determined using $\Delta t=0.01$ ps and $M=10^4$ realizations.

The simulations show good agreement with the analytical results for the given parameters ($\gamma = 0.5\ \text{THz}$, $I = 1$, $\nu_0 = 10\ \text{THz}$, $\Delta t = 0.01\ \text{ps}$, $M = 10^4$).

2.3. Modelling of Emission Shapes

The emission of a diode (1) is described as the superposition of N independent classical fields with individual linewidths γ_j, mean intensities I_j and central frequencies ν_j. The stationary first-order temporal correlation function reads

$$G_{\text{d}}^{(1)}(\tau) = \lim_{t\to\infty}\left\langle \varepsilon_{\text{d}}^{*}(t)\,\varepsilon_{\text{d}}(t+\tau)\right\rangle = \lim_{t\to\infty}\sum_{j=1}^{N}\left\langle \varepsilon_j^{*}(t)\,\varepsilon_j(t+\tau)\right\rangle. \tag{11}$$

Thus, the spectral power density is the incoherent sum of the individual spectra

$$S_{\text{d}}(\nu) = \sum_{j=1}^{N} S_j(\nu). \tag{12}$$

This model can be used to approximate a wide range of shapes through the adjustment of the 3 N free parameters γ_j, I_j and ν_j in (12) by means of a least square fit, minimizing the error functional

$$e = \sum_i \left(S_{\text{t}}(\nu_i) - S_{\text{d}}(\nu_i)\right)^2 \tag{13}$$

for a test spectrum $S_{\text{t}}(\nu)$ at discrete frequencies ν_i. Examples of interest are given by Gaussian spectra [39]

$$S_{\text{g}}(\nu) = \frac{1}{\sqrt{\sigma^2}}\,\text{e}^{-\frac{(\nu-\nu_0)^2}{2\sigma^2}}, \tag{14}$$

Lorentzian spectra [39]

$$S_{\text{l}}(\nu) = \sqrt{\frac{2}{\pi}}\,\frac{\gamma}{(\nu-\nu_0)^2+\gamma^2}, \tag{15}$$

Voigt profiles [39]

$$S_{\text{v}}(\nu) = \frac{1}{\sqrt{\sigma^2}}\,\text{Re}\left\{\text{e}^{-z^2}\,\text{erfc}(-\text{i}z)\right\},\quad z = \frac{\nu+\text{i}\gamma}{\sigma\sqrt{2}}, \tag{16}$$

with the complementary error function $\text{erfc}(z)$, and bandwidth limited box shapes

$$S_{\text{b}}(\nu) = \begin{cases} \sqrt{2\pi}/\gamma, & \text{for } |\nu| \le \gamma/2, \\ 0, & \text{else.} \end{cases} \tag{17}$$

This is illustrated in **Figure 2**. Please note that all spectra are normalized to

$$\frac{1}{\sqrt{2\pi}}\int_{-\infty}^{\infty} \text{d}\nu\, S(\nu) = 1. \tag{18}$$

2.4. Model of Quantum Dot Superluminescent Diode Emission

Superluminescent diodes are semiconductor-based light sources, which are characterized by spatially directed emission and spectral widths in the THz regime. The experiments with QDSLDs [3] had an active medium consisting of inhomogeneously broadened InAs/InGaAs quantum dot layers. The optical power spectrum has a Gaussian shape (see **Figure 3**).

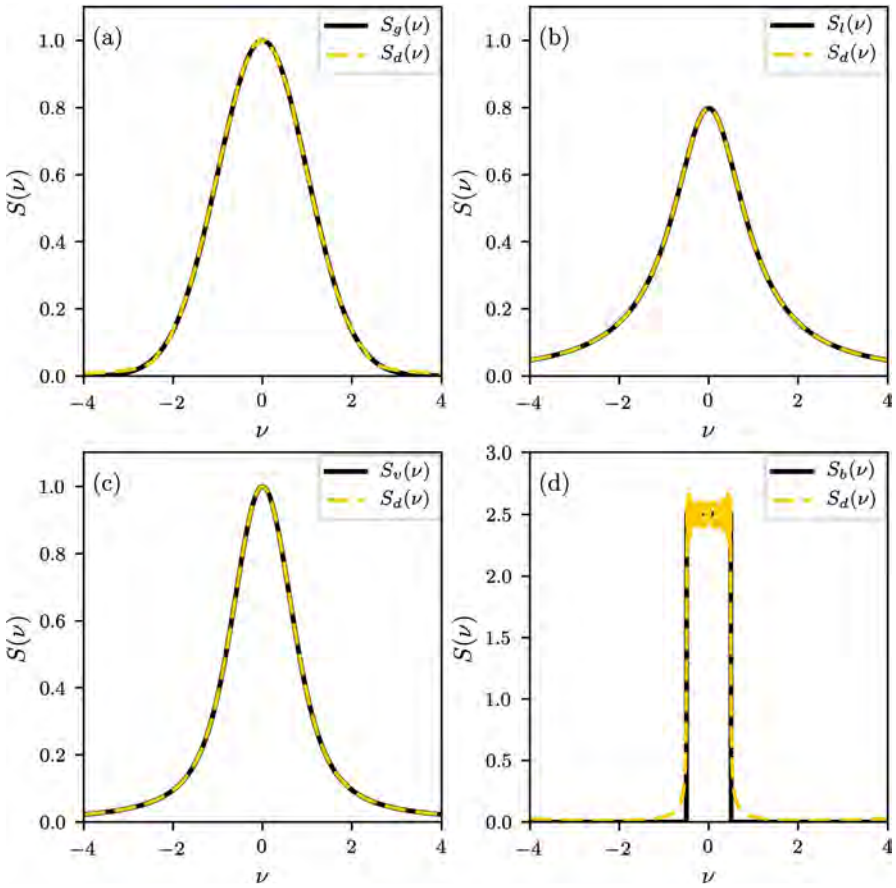

Figure 2. (a) Gaussian spectrum $S_g(\nu)$, (b) Lorentzian spectrum $S_l(\nu)$, (c) Voigt profile $S_v(\nu)$ and (d) bandwidth limited box shape $S_b(\nu)$ versus frequency ν (black, solid; $\nu_0 = 0$, $\sigma = 1$, $\gamma = 1$) modelled according to (12) with $N = 30$ elementary oscillators (yellow, dashed). The oscillations at the edge of the box are a typical Gibbs phenomenon [40].

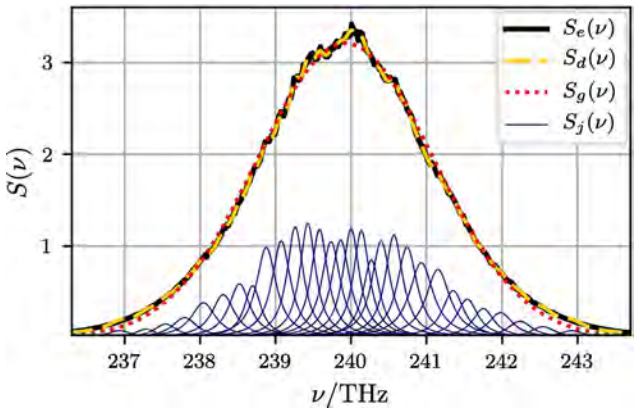

Figure 3. Experimental optical power spectrum $S_e(\nu)$ (black, solid) versus frequency ν [3] with Gaussian fit $S_g(\nu)$ (red, dotted), stochastic emission $S_d(\nu)$ for $N = 30$ oscillators according to (12) (yellow, dashed) and spectra of individual oscillators $S_j(\nu)$ (solid, blue). The results of the Gaussian fit are a central frequency $\nu_0 = 239.9$ THz and a width $\sigma = 1.17$ THz.

Therefore the developed formalism is used to describe the emission of the diode, which is modelled by $N = 30$ individual oscillators. Using a least square fit (see (13)) to an experimental spectrum $S_e(\nu)$ [3] the linewidths γ_j, mean intensities I_j and central frequencies ν_j describing the emission are determined. This is illustrated in Figure 3.

3. QDSLD Emission Spectrum

The optical power spectrum emitted by the QDSLD is simulated numerically. For this, the central frequencies ν_j, linewidths γ_j and mean intensities I_j describing the QDSLD emission determined in Sec. 2.4 are used to calculate the individual electric fields $\varepsilon_j(t)$ according to (8). The electric field emitted by the diode $\varepsilon_d(t)$ results as a superposition of the individual field $\varepsilon_j(t)$ according to (1). Subsequently, the stationary first-order temporal correlation function $G_d^{(1)}(\tau)$ is calculated according to (9) using $M = 10^4$ realizations of the diode field $\varepsilon_d(t)$. The spectral power density of the emission $S_d(\nu)$ is determined using a Fourier transformation.

The result of the simulation (see Figure 4) shows good agreement with the experimental optical power spectrum [3]. We define the width of the spectral power density [41] [42]

$$b = \frac{1}{\int_{-\infty}^{\infty} \mathrm{d}\nu\, S^2(\nu)}. \tag{19}$$

This yields $b_d = 4.51$ THz, implying a coherence time of $\tau_{c,d} = 1/b_d = 221.9$ fs, which matches the experimental results of $b_e = 4.29$ THz and $\tau_{c,e} = 233$ fs very well.

The method of modelling emission spectra as a superposition of individual oscillators is therefore suitable to describe the first-order temporal correlation properties of QDSLDs.

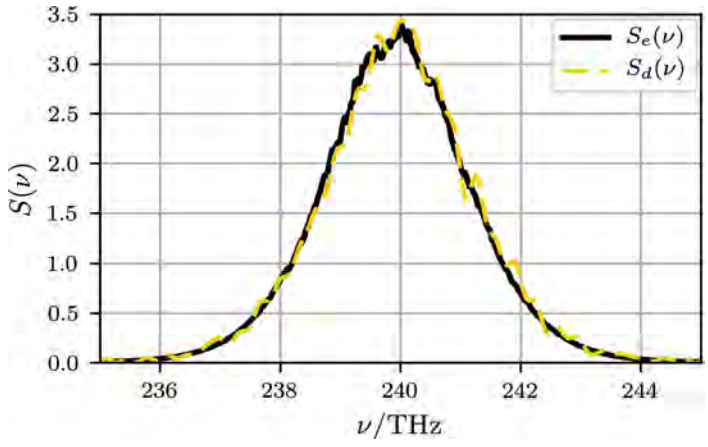

Figure 4. Experimental optical power spectrum $S_e(\nu)$ (black, solid) versus frequency ν [3] with simulation results $S_d(\nu)$ (yellow, dashed) for $N = 30$ oscillators resulting from a Fourier transformation of the stationary first-order temporal correlation function $G_d^{(1)}(\tau)$ calculated according to (9) with $M = 10^4$.

By extracting appropriate simulation parameters from an experimental spectrum, the electric field emitted by the diode can be simulated numerically and can be used to calculate the stationary first-order temporal correlation function and optical power spectrum of the emission.

4. Second-Order Temporal Correlation Function

In addition to the investigation of the optical power spectrum, the developed formalism can be used to investigate the classical photon statistics of the QDSLD emission. For this, the electric field $\varepsilon_{\mathrm{d}}(t)$ emitted by the diode already calculated in Sec. 3 can be reused. Instead of calculating first-order temporal correlation properties of the field, M realizations of $\varepsilon_{\mathrm{d}}(t)$ are used to calculate the stationary normalized second-order temporal correlation function $g_{\mathrm{d}}^{(2)}(\tau)$ of the emission according to (6, 9, 10).

The result for the central frequencies ν_j, linewidths γ_j and mean intensities I_j determined in Section 2.4 is illustrated in Figure 5. There is good agreement between the simulation and the experimental data $g_{\mathrm{e}}^{(2)}(\tau)$. The central degree of second-order temporal coherence $g_{\mathrm{d}}^{(2)}(\tau=0)\simeq 2$ indicates a Gaussian photon distribution, which was also shown experimentally. Therefore, the developed formalism is suited for classical photon statistical investigations of QDSLDs.

5. Conclusions

In this article, we study a stochastic model to describe experimental emission spectra. These are considered to result as a superposition of individual complex Ornstein-Uhlenbeck processes. The first- and second-order temporal correlation properties of these oscillators are investigated analytically and numerically. We can approximate Gaussian-, Lorentzian-, Voigt- and bandwidth limited spectra by determination of Lorentzian linewidths, carrier frequencies and amplitudes of the individual oscillators using least square fits.

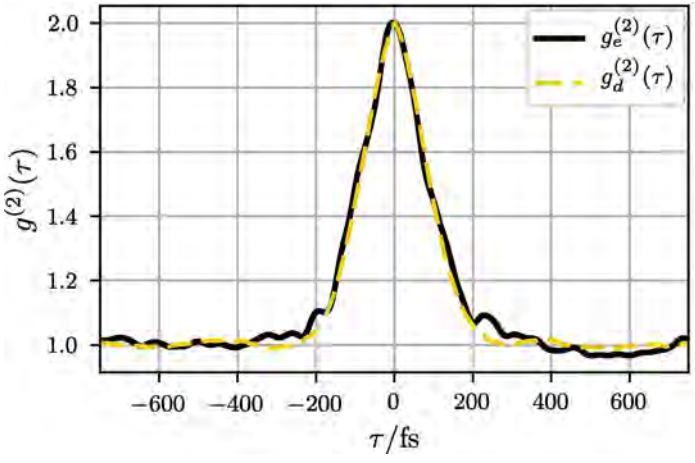

Figure 5. Experimental stationary normalized second-order temporal correlation function $g_{\mathrm{e}}^{(2)}(\tau)$ (black, solid) versus time τ [3] with simulation results $g_{\mathrm{d}}^{(2)}(\tau)$ (yellow, dashed) for $N=30$ oscillators calculated according to (9, 10) with $M=10^4$.

The developed procedure is applied to the emission properties of quantum dot superluminescent diodes. Simulation parameters are extracted from a least square fit to an experimental spectrum [3]. These are used to simulate the QDSLD emission and calculate first- and second-order temporal correlation properties. The determined spectral power density of the emission, resulting from a Fourier transformation of the stationary first-order temporal correlation function, shows good agreement with the experimental results regarding the shape of the spectral line, as well as spectral width and coherence time. Additionally, calculating the stationary normalized second-order temporal correlation function results in a central degree of second-order temporal coherence $g^{(2)}(\tau = 0) \simeq 2$. This indicates a Gaussian photon distribution, which is in agreement with experiments and former theoretical investigations.

The stochastic description of QDSLD emission offers a straightforward perspective on the process of light generation inside QDSLDs, describing it as a superposition of individual classical oscillators. More data on the emission characteristics of the constituents of QDSLDs can lead to a better understanding and contribute to the design of new diodes. Furthermore, this approach can be utilized in the investigation of other properties of QDSLDs. As it explains the statistical properties of the electric field emitted by the diode, it can be used in a classical explanation of temperature dependent intensity fluctuation suppression observed by Blazek *et al.*

Acknowledgements

We thank Sébastien Blumenstein for the provision of experimental data and Prof. Wolfgang Elsäßer for stimulating discussions.

Conflicts of Interest

The authors declare no conflicts of interest regarding the publication of this paper.

References

[1] Huang, D., Swanson, E.A., Lin, C.P., Schuman, J.S., Stinson, W.G., Chang, W., Hee, M.R., Flotire, T., Gregory, K., Puliafito, C.A. and Fujimoto, J.G. (1991) *Science*, **22**, 1178-1181. https://doi.org/10.1126/science.1957169

[2] Judson, P.D.L., Groom, K.M., Childs, D.T.D., Hopkinson, M., Krstajic, N. and Hogg, R.A. (2009) *Microelectronics Journal*, **40**, 588-591. https://doi.org/10.1016/j.mejo.2008.06.037

[3] Hartmann, S. and Elsäßer, W. (2017) *Journal of Modern Optics*, **7**, Article No. 41866. https://doi.org/10.1038/srep41866

[4] Pittman, T.B., Shih, Y.H., Strekalov, D.V. and Sergienko, A.V. (1995) *Physical Review A*, **52**, R3429-R3432. https://doi.org/10.1103/PhysRevA.52.R3429

[5] Gatti, A., Bache, M., Magatti, D., Brambilla, E., Ferri, F. and Lugiato, L.A. (2006) *Journal of Modern Optics*, **53**, 739-760. https://doi.org/10.1080/09500340500147240

[6] Lee, T.-P., Burrus, C.A. and Miller, B.I. (1973) *IEEE Journal of Quantum Electron-*

ics, **QE-9**, 820-828. https://doi.org/10.1109/JQE.1973.1077738

[7] Boitier, F., Godard, A., Rosencher, E. and Fabre, C. (2009) *Nature Physics*, **5**, 267-270. https://doi.org/10.1038/nphys1218

[8] Uskov, A.V., Berg, T.W. and Mørk, J. (2004) *IEEE Journal of Quantum Electronics*, **40**, 306-320. https://doi.org/10.1109/JQE.2003.823032

[9] Bardella, P., Rossetti, M. and Montrosset, I. (2009) *IEEE Journal of Selected Topics in Quantum Electronics*, **15**, 785-791. https://doi.org/10.1109/JSTQE.2009.2013128

[10] Forrest, A.F., Krakowski, M., Bardella, P. and Cataluna, M.A. (2020) *Optics Express*, **28**, 846-859. https://doi.org/10.1364/OE.377768

[11] Rossetti, M., Bardella, P. and Montrosset, I. (2011) *IEEE Journal of Quantum Electronics*, **47**, 139-150. https://doi.org/10.1109/JQE.2010.2055550

[12] Li, Z.Q. and Li, Z.M.S. (2010) *IEEE Journal of Quantum Electronics*, **46**, 454-461. https://doi.org/10.1109/JQE.2009.2032426

[13] Friedrich, F., Elsäßer, W. and Walser, R. (2020) *Optics Communications*, **458**, Article ID: 124449. https://doi.org/10.1016/j.optcom.2019.124449 http://www.sciencedirect.com/science/article/pii/S0030401819307515

[14] Hartmann, S., Friedrich, F., Molitor, A., Reichert, M., Elsäßer, W. and Walser, R. (2015) *New Journal of Physics*, **17**, Article ID: 043039. https://doi.org/10.1088/1367-2630/17/4/043039

[15] Jechow, A., Seefeldt, M., Kurzke, H., Heuer, A. and Menzel, R. (2013) *Nature Photonics*, **7**, 973-976. https://doi.org/10.1038/nphoton.2013.271

[16] Kiethe, J., Heuer, A. and Jechow, A. (2017) *Laser Physics Letters*, **14**, Article ID: 086201. http://stacks.iop.org/1612-202X/14/i=8/a=086201 https://doi.org/10.1088/1612-202X/aa772c

[17] Blazek, M. and Elsäßer, W. (2011) *Physical Review A*, **84**, Article ID: 063840. https://doi.org/10.1103/PhysRevA.84.063840

[18] Ozaki, N., Yamauchi, S., Hayashi, Y., Watanabe, E., Ohsato, H., Ikeda, N., Sugimoto, Y., Furuki, K., Oikawa, Y., Miyaji, K., Childs, D.T.D. and Hogg, R.A. (2019) *Journal of Physics D: Applied Physics*, **52**, Article ID: 225105. https://doi.org/10.1088/1361-6463/ab0ea5

[19] Forrest, A.F., Krakowski, M., Bardella, P. and Cataluna, M.A. (2019) *Optics Express*, **27**, 10981-10990. https://doi.org/10.1364/OE.27.010981

[20] Aho, A.T., Viheriälä, J., Virtanen, H., Zia, N., Isoaho, R. and Guina, M. (2009) *Applied Physics Letters*, **115**, Article ID: 081104. https://doi.org/10.1063/1.5111012

[21] Brückner, D.B., Fink, A., Schreiber, C., Röttgermann, P.J.F., Rädler, J.O. and Broedersz, C.P. (2019) *Nature Physics*, **15**, 595-601. https://doi.org/10.1038/s41567-019-0445-4

[22] Fang, X., Kruse, K., Lu, T. and Wang, J. (2019) *Reviews of Modern Physics*, **91**, Article ID: 045004. https://doi.org/10.1103/RevModPhys.91.045004

[23] Vagne, Q. and Sens, P. (2018) *Physical Review Letters*, **120**, Article ID: 058102. https://doi.org/10.1103/PhysRevLett.120.058102

[24] Nesti, T., Zocca, A. and Zwart, B. (2018) *Physical Review Letters*, **120**, Article ID: 258301. https://doi.org/10.1103/PhysRevLett.120.258301

[25] Kanazawa, K., Sueshige, T., Takayasu, H. and Takayasu, M. (2018) *Physical Review Letters*, **120**, Article ID: 138301. https://doi.org/10.1103/PhysRevLett.120.138301

[26] Hartmann, M.J. and Carleo, G. (2019) *Physical Review Letters*, **122**, Article ID: 250502. https://doi.org/10.1103/PhysRevLett.122.250502

[27] Yoshioka, N. and Hamazaki, R. (2019) *Physical Review B*, **99**, Article ID: 214306. https://doi.org/10.1103/PhysRevB.99.214306

[28] Qi, K., Westphal, E., Gompper, G. and Winkler, R.G. (2020) *Physical Review Letters*, **124**, Article ID: 068001. https://doi.org/10.1103/PhysRevLett.124.068001

[29] Liebchen, B. and Löwen, H. (2019) *The Journal of Chemical Physics*, **150**, Article ID: 061102. https://doi.org/10.1063/1.5082284

[30] Walser, R., Cooper, J. and Zoller, P. (1994) *Physical Review A*, **50**, 4304. https://doi.org/10.1103/PhysRevA.50.4303

[31] McIntyre, D., Fairchild, C., Cooper, J. and Walser, R. (1993) *Optics Letters*, **18**, 1816-1818. https://doi.org/10.1364/OL.18.001816

[32] Uhlenbeck, G.E. and Ornstein, L.S. (1930) *Physical Review*, **36**, 823-841. https://doi.org/10.1103/PhysRev.36.823

[33] Gardiner, C. (2009) Stochastic Methods: A Handbook for the Natural and Social Sciences. Springer, Berlin.

[34] Glauber, R.J. (1963) *Physical Review*, **130**, 2529. https://doi.org/10.1103/PhysRev.130.2529

[35] Wiener, N. (1930) *Acta Mathematica*, **55**, 117-258. https://doi.org/10.1007/BF02546511

[36] Khintchine, A. (1934) *Mathematische Annalen*, **109**, 604-615. https://doi.org/10.1007/BF01449156

[37] Mandel, L. and Wolf, E. (1995) Optical Coherence and Quantum Optics. Cambridge Univeristy Press, Cambridge. https://doi.org/10.1017/CBO9781139644105

[38] Kloeden, P.E. and Platen, E. (1999) Numerical Solution of Stochastic Differential Equations. Springer, Berlin.

[39] Olver, F.W.J., Olde Daalhuis, A.B., Lozier, D.W., Schneider, B.I., Boisvert, R.F., Clark, C.W., Miller, B.R., Saunders, B.V., Cohl, H.S. and McClain, M.A. (2020) NIST Digital Library of Mathematical Functinos, Release 1.0.28 of 2020-09-15. http://dlmf.nist.gov

[40] Jerri, A.J. (1998) The Gibbs Phenomenon in Fourier Analysis, Splines and Wavelet Approximations. Springer US, New York. https://doi.org/10.1007/978-1-4757-2847-7

[41] Süßmann, G. (1997) *Zeitschrift für Naturforschung*, **52**, 49-52. https://doi.org/10.1515/zna-1997-1-214

[42] Schleich, W.P. (2011) Quantum Optics in Phase Space. Wiley, Berlin.

[43] Milstein, G.N. (1975) *Theory of Probability and Its Applications*, **19**, 557-562. https://doi.org/10.1137/1119062

Appendix. Convergence of Stochastic Simulations

Consider the Ito stochastic differential equation [33]

$$\mathrm{d}x(t) = a\big(x(t)\big)\mathrm{d}t + b\big(x(t)\big)\mathrm{d}W(t), \tag{20}$$

with the drift term $a(x)$ and the diffusion term $b(x)$. Identifying $x(t_0) = x_0$, the formal solution of this equation is given by integration:

$$x(t) = x_0 + \int_{t_0}^{t} \mathrm{d}t' a\big(x(t')\big) + \int_{t_0}^{t} \mathrm{d}W(t') b\big(x(t')\big) \tag{21}$$

The goal of time discrete maps $x(t_{i+1}) = F(x_i)$ of stochastic differential equations is the approximation of a solution $x(t)$ up to a order of convergence γ. Such a scheme is said to converge strongly with order $\gamma > 0$, if for the final time instant T and $N = T/\Delta$ there is a finite ε and $\Delta_0 > 0$ such that [38]

$$\Big\langle \big| x(T) - x(t_N) \big| \Big\rangle \le \varepsilon \Delta^{\gamma} \tag{22}$$

for any time discretization $0 < \Delta < \Delta_0$. A strong Taylor scheme of order γ can be constructed by considering the Ito-Taylor expansion, which is obtained by continuously applying the integral form of Ito's formula [33]

$$f\big(x(t)\big) = f(x_0) + \int_{t_0}^{t} \mathrm{d}t' L^0 f\big(x(t')\big) + \int_{t_0}^{t} \mathrm{d}W(t') L^1 f\big(x(t')\big), \tag{23}$$

with $L^0 = a\big(x(t')\big)\partial_x + (1/2)b^2\big(x(t')\big)\partial_x^2$ and $L^1 = b\big(x(t')\big)\partial_x$, to nonconstant terms inside the integrals of the formal solution (21). A criterium [38] for the terms of the Ito-Taylor expansion required for the associated strong Taylor scheme to achieve a desired order of strong convergence γ states, that a simulation scheme strongly converges to the order of an integer γ if it includes all combinations of integrals up to this order, with time differentials $\mathrm{d}t$ being of order 1 and Wiener noise increments $\mathrm{d}W(t)$ being of order 1/2. Simulation schemes of half-integer order γ additionally require the inclusion of the pure time integral of order $\gamma + 1/2$.

A strong convergence scheme of order 1/2 is the Euler scheme

$$x(t) = x_0 + a(x_0)\int_{t_0}^{t} \mathrm{d}t' + b(x_0)\int_{t_0}^{t} \mathrm{d}W(t') + \mathcal{R}. \tag{24}$$

Discretizing the time steps, discrete map can be developed which yields

$$x(t_{i+1}) = x(t_i) + a\big(x(t_i)\big)\Delta t + b\big(x(t_i)\big)\Delta W, \tag{25}$$

where ΔW is a Gaussian random process with $\langle \Delta W \rangle = 0$ and $\langle \Delta W^2 \rangle = \Delta t$. To expand the Euler scheme to order 1.0 of strong convergence, the double stochastic integral appearing in the remainder $\mathcal{R}$ in (24) has to be included, yielding

$$x(t) = x_0 + a(x_0)\int_{t_0}^{t} \mathrm{d}t' + b(x_0)\int_{t_0}^{t} \mathrm{d}W(t') + L^1 b(x_0)\int_{t_0}^{t}\int_{t_0}^{t'} \mathrm{d}W(t')\mathrm{d}W(t'') + \mathcal{R}. \tag{26}$$

This is called the Milstein scheme [43]. The double stochastic integral can be calculated [33]

$$\int_{t_0}^{t}\int_{t_0}^{t'} \mathrm{d}W(t')\mathrm{d}W(t'') = \frac{1}{2}\Big[\big(W(t) - W(t_0)\big)^2 - (t - t_0)\Big], \tag{27}$$

which leads to the iteration rule for the Milstein method

$$x(t_{i+1}) = x(t_i) + \left[a(x(t_i)) - \frac{1}{2} b(x(t_i)) \partial_x b(x(t_i)) \right] \Delta t + b(x(t_i)) \Delta W + \frac{1}{2} b(x(t_i)) \partial_x b(x(t_i)) \Delta W^2. \tag{28}$$

With increasing order of convergence γ, the simulation schemes become more complex and include an increasing number of stochastic increments.

Journal of Modern Physics, 2021, 12, 35-49
https://www.scirp.org/journal/jmp
ISSN Online: 2153-120X
ISSN Print: 2153-1196

Bound States of a System of Two Fermions on Invariant Subspace

J. I. Abdullaev, A. M. Toshturdiev*

Samarkand State University, University Boulevard 15, Samarkand, Uzbekistan
Email: jabdullaev@mail.ru, *atoshturdiyev@mail.ru

How to cite this paper: Abdullaev, J.I. and Toshturdiev, A.M. (2021) Bound States of a System of Two Fermions on Invariant Subspace. *Journal of Modern Physics*, **12**, 35-49.
https://doi.org/10.4236/jmp.2021.121004

Received: October 26, 2020
Accepted: January 11, 2021
Published: January 14, 2021

Abstract

We consider a Hamiltonian of a system of two fermions on a three-dimensional lattice $\mathbb{Z}^3$ with special potential $\hat{v}$. The corresponding Shrödinger operator $H(\mathbf{k})$ of the system has an invariant subspace $L_{123}^{-}(\mathbb{T}^3)$, where we study the eigenvalues and eigenfunctions of its restriction $H_{123}^{-}(\mathbf{k})$. Moreover, there are shown that $H_{123}^{-}(k_1,k_2,\pi)$ has also infinitely many invariant subspaces $\mathfrak{R}_{123}^{-}(n), n\in\mathbb{N}$, where the eigenvalues and eigenfunctions of eigenvalue problem

$$H(k_1,k_2,\pi)f = zf,\quad f\in\mathfrak{R}_{123}^{-}(n)$$

are explicitly found.

Keywords

Hamiltonian, Fermion, Bound State, Shrödinger Operator, Invariant Subspace, Total Quasi-Momentum, Eigenvalue, Birman-Schwinger Principle

1. Introduction

The nature of bound states of two-particle cluster operators for small parameter values was first studied in detail by Minlos and Mamatov [1] and then in a more general setting by Minlos and Mogilner [2]. In [3], Howland showed that the Rellich theorem on perturbations of eigenvalues does not extend to the resonance theory. Studying bound states of a two-particle system Hamiltonian H on the d-dimensional lattice $\mathbb{Z}^d$ reduces to studying [2] [4] [5] [6] [7] the eigenvalues of a family of Shrödinger operators $H(\mathbf{k}), \mathbf{k}\in\mathbb{T}^d$, where $\mathbf{k}$ is the total quasi-momentum of a system. Moreover, eigenfunctions of $H(\mathbf{k})$ are interpreted as bound states of the Hamiltonian H, and eigenvalues, as the bound state

energies. The bound states of H of a system of two fermions on a one-dimensional lattice were studied in [4], a system of two bosons on a two-dimensional lattice was studied in [6], and perturbations of the eigenvalues of a two-particle Shrödinger operator on a one-dimensional lattice were studied in [8]. The finiteness of the number of eigenvalues of Shrödinger operator on a lattice was studied in the works [7] [9].

The discrete spectrum of the two-particle continuous Shrödinger operator

$$h_\lambda = -\Delta + \lambda V$$

was studied by many authors, with the conditions for the potential V formulated in its coordinate representation. The condition for the finiteness of the set of negative elements of the spectrum and the absence of positive eigenvalues of h_λ can be found in [10]. If $V \le 0$, then the number of negative eigenvalues $N(\lambda)$ is a nondecreasing function of $\lambda \in (0,\infty)$, and each eigenvalue $z_n(\lambda)$ decreases on the half-axis $(0,\infty)$. It is known that when the coupling constant λ decreases, the bound state energies of h_λ tend to the boundary of the continuous spectrum (see [10]) and for some finite λ are on the boundary. Two questions then arise: Does a bound or virtual state correspond to such a threshold state (*i.e.*, is the corresponding wave function square-integrable)? And where do the bound states "disappear to" as λ decreases further? The study of the first question was the subject in [11] [12]. Regarding the second question, it turns out that the bound state disappears by being absorbed into the continuous spectrum and becomes a resonance [5].

Here, we consider bound states of the Hamiltonian $\hat{H}$ (see (1)) of a system of two fermions on the three-dimensional lattice $\mathbb{Z}^3$ with the special potential $\hat{v}$ (see (5)). In other words, we study the discrete spectrum of a family of the Shrödinger operators $H(\mathbf{k})$, $\mathbf{k} = (k_1, k_2, k_3) \in \mathbb{T}^3$, (see (3)) corresponding to $\hat{H}$ in the invariant subspace $L_{123}^-(\mathbb{T}^3)$.

Restriction of the operator $H(\mathbf{k})$ in the invariant subspace $L_{123}^-(\mathbb{T}^3)$ is denoted by $H_{123}^-(\mathbf{k})$.

In the case $\mathbf{k} = \vec{\pi} := (\pi, \pi, \pi)$, the operator $H(\vec{\pi})$ has an infinite number of eigenvalues of the form $6 - \hat{v}(\mathbf{n}), \mathbf{n} \in \mathbb{Z}^3$ and the essential spectrum consists of the single point 6. Here, the potential $\hat{v}$ is defined by (5) and $\overline{v} : \mathbb{N} \to \mathbb{R}$ is a decreasing function on $\mathbb{N}$ and $\overline{v} \in \ell_2(\mathbb{N})$. These eigenvalues $z_n(\vec{\pi}) = 6 - \overline{v}(n), n \in \mathbb{N}$ are arranged in ascending order, $z_1(\vec{\pi}) < \cdots < z_n(\vec{\pi}) < \cdots$, and the smallest eigenvalue $z_1(\vec{\pi}) = 6 - \overline{v}(1)$ is threefold, $z_2(\vec{\pi}) = 6 - \overline{v}(2)$ is sevenfold, and the other eigenvalues $z_n(\vec{\pi}) = 6 - \overline{v}(n), n \ge 3$ are ninefold. All ninefold eigenvalues $z_n(\vec{\pi}) = 6 - \overline{v}(n), n \ge 3$ of the operator $H(\vec{\pi})$ are simple eigenvalues for the operator $H_{123}^-(\vec{\pi})$.

Further, we investigate eigenvalues and eigenfunctions of the restriction operator $H_{123}^-(\mathbf{k})$.

In the case $\mathbf{k} = (k_1, k_2, \pi)$ the corresponding operator $H_{123}^-(k_1, k_2, \pi)$ has infinitely many invariant subspaces $\mathfrak{R}_{123}^-(n) := L_2^-(\mathbb{T}) \otimes L_2^-(\mathbb{T}) \otimes L^-(n), n \in \mathbb{N}$. It

is proved that the restriction $H_{123n}^{-}(k_1,k_2,\pi)$ of the operator $H_{123}^{-}(k_1,k_2,\pi)$ in the invariant subspace $\Re_{123}^{-}(n)$ has no more than one eigenvalue. If exists, it can be calculated explicitly. For every $(k_1,k_2)\in(-\pi,\pi)^2$ the operator $H_{123}^{-}(k_1,k_2,\pi)$ has only a finite number of eigenvalues.

For any perturbation $\beta>0$, the essential spectrum $\{6\}$ of $H(\vec{\pi})$ becomes the essential spectrum $\sigma_{ess}(H(\pi-2\beta,\pi,\pi))=[6-2\sin\beta,6+2\sin\beta]$. If the potential $\hat{v}$ is of the form (5), the Shrödinger equation $H_{123}^{-}(\pi-2\beta,\pi,\pi)f=zf$, $f\in\Re_{123}^{-}(n)$ can be exactly solved (see Theorem 1).

The Shrödinger equations $H(\pi-2\beta,\pi,\pi)f=zf$ and $H(\pi-2\beta,\pi-2\beta,\pi)f=zf$, $f\in\Re_{123}^{-}(n)$ with small β are solved by using methods invariant subspaces and operator theory.

2. Description of the Hamiltonian and Expansion in a Direct Integral

The free Hamiltonian $\hat{H}_0$ of a system of two fermions on a three-dimensional lattice $\mathbb{Z}^3$ usually corresponds to a bounded self-adjoint operator acting in the Hilbert space $\ell_2^{as}(\mathbb{Z}^3\times\mathbb{Z}^3):=\{f\in\ell_2(\mathbb{Z}^3\times\mathbb{Z}^3): f(\mathbf{x},\mathbf{y})=-f(\mathbf{y},\mathbf{x})\}$ by the formula

$$\hat{H}_0=-\frac{1}{2m}\Delta_1-\frac{1}{2m}\Delta_2.$$

Here, m is the fermion mass, which we assume to be equal to unity in what follows, $\Delta_1=\Delta\otimes I$ and $\Delta_2=I\otimes\Delta$, where I is the identity operator, and the lattice Laplacian Δ is a difference operator that describes a translation of a particle from a side to a neighboring side,

$$(\Delta\hat{\psi})(\mathbf{x})=\sum_{j=1}^{3}\left[\hat{\psi}(\mathbf{x}+\mathbf{e}_j)+\hat{\psi}(\mathbf{x}-\mathbf{e}_j)-2\hat{\psi}(\mathbf{x})\right],\ \mathbf{x}\in\mathbb{Z}^3,\ \hat{\psi}\in\ell_2(\mathbb{Z}^3),$$

where $\mathbf{e}_1=(1,0,0),\mathbf{e}_2=(0,1,0),\mathbf{e}_3=(0,0,1)$ are unit vectors in $\mathbb{Z}^3$. The total Hamiltonian $\hat{H}$ acts in the Hilbert space $\ell_2^{as}(\mathbb{Z}^3\times\mathbb{Z}^3)$ and is the difference of the free Hamiltonian $\hat{H}_0$ and the interaction potential $\hat{V}_2$ of the two fermions (see [8] [13]):

$$\hat{H}=\hat{H}_0-\hat{V}_2, \tag{1}$$

where

$$(\hat{V}_2\hat{\psi})(\mathbf{x},\mathbf{y})=\hat{v}(\mathbf{x}-\mathbf{y})\hat{\psi}(\mathbf{x},\mathbf{y}),\quad \hat{\psi}\in\ell_2^{as}\left(\left(\mathbb{Z}^3\right)^2\right):=\ell_2^{as}(\mathbb{Z}^3\times\mathbb{Z}^3).$$

Hereafter, we assume that

$$\hat{v}\in\ell_2(\mathbb{Z}^3)\ \text{ and }\ \hat{v}(\mathbf{x})=\hat{v}(-\mathbf{x})\geq 0\quad \text{for all } \mathbf{x}\in\mathbb{Z}^3. \tag{2}$$

Under this condition, the Hamiltonian $\hat{H}$ is a bounded self-adjoint operator in $\ell_2^{as}\left(\left(\mathbb{Z}^3\right)^2\right)$.

We pass to momentum representation using the Fourier transform [2] [4] [7]

$$F:\ell_2^{as}(\mathbb{Z}^3\times\mathbb{Z}^3)\to L_2^{as}(\mathbb{T}^3\times\mathbb{T}^3).$$

The Hamiltonian $H = H_0 - V = F\hat{H}F^{-1}$ in the momentum representation commutes with the unitary operators $U_{\mathbf{s}}, \mathbf{s} \in \mathbb{Z}^3$, given by

$$\left(U_{\mathbf{s}} f\right)\left(\mathbf{k}_1, \mathbf{k}_2\right) = \exp\left(-i\left(\mathbf{s}, \mathbf{k}_1 + \mathbf{k}_2\right)\right) f\left(\mathbf{k}_1, \mathbf{k}_2\right), \quad f \in L_2^{as}\left(\mathbb{T}^3 \times \mathbb{T}^3\right).$$

It follows that there exist decompositions of $L_2^{as}\left(\mathbb{T}^3 \times \mathbb{T}^3\right)$ and the operators $U_{\mathbf{s}}$ and H into direct integrals (see [7] [9] and [10])

$$L_2^{as}\left(\mathbb{T}^3 \times \mathbb{T}^3\right) = \int_{\mathbb{T}^3} \oplus L_2^{as}\left(F_{\mathbf{k}}\right) \mathrm{d}\mathbf{k}, \; U_{\mathbf{s}} = \int_{\mathbb{T}^3} \oplus U_{\mathbf{s}}\left(\mathbf{k}\right) \mathrm{d}\mathbf{k}, \; H = \int_{\mathbb{T}^3} \oplus \tilde{H}\left(\mathbf{k}\right) \mathrm{d}\mathbf{k}.$$

Here,

$$F_{\mathbf{k}} = \left\{\left(\mathbf{k}_1, \mathbf{k}_2\right) \in \mathbb{T}^3 \times \mathbb{T}^3 : \mathbf{k}_1 + \mathbf{k}_2 = \mathbf{k}\right\}, \quad \mathbf{k} \in \mathbb{T}^3,$$

and $U_{\mathbf{s}}\left(\mathbf{k}\right)$ is an operator of multiplication by the function $\exp\left(-i\left(\mathbf{s}, \mathbf{k}\right)\right)$ in $L_2^{as}\left(F_{\mathbf{k}}\right)$. The fiber operator $\tilde{H}\left(\mathbf{k}\right)$ of H also acts in $L_2^{as}\left(F_{\mathbf{k}}\right)$ and is unitarly equivalent to $H\left(\mathbf{k}\right) := H_0\left(\mathbf{k}\right) - V$, which is called the Shrödinger operator. This operator acts in the Hilbert space $L_2^o\left(\mathbb{T}^3\right) := \left\{f \in L_2\left(\mathbb{T}^3\right) : f\left(-\mathbf{q}\right) = -f\left(\mathbf{q}\right)\right\}$ by the formula

$$\left(H\left(\mathbf{k}\right) f\right)\left(\mathbf{q}\right) = \varepsilon_{\mathbf{k}}\left(\mathbf{q}\right) f\left(\mathbf{q}\right) - \left(2\pi\right)^{-\frac{3}{2}} \int_{\mathbb{T}^3} v\left(\mathbf{q} - \mathbf{s}\right) f\left(\mathbf{s}\right) \mathrm{d}\mathbf{s}. \tag{3}$$

The unperturbed operator $H_0\left(\mathbf{k}\right)$ is an operator of multiplication by the function

$$\begin{aligned} \varepsilon_{\mathbf{k}}\left(\mathbf{q}\right) &= \varepsilon\left(\frac{\mathbf{k}}{2} + \mathbf{q}\right) + \varepsilon\left(\frac{\mathbf{k}}{2} - \mathbf{q}\right) \\ &= 6 - 2\cos\frac{k_1}{2}\cos q_1 - 2\cos\frac{k_2}{2}\cos q_2 - 2\cos\frac{k_3}{2}\cos q_3. \end{aligned} \tag{4}$$

From (3) and (4), it follows that

$$H\left(k_1, k_2, k_3\right) = H\left(-k_1, k_2, k_3\right) = H\left(k_1, -k_2, k_3\right) = H\left(k_1, k_2, -k_3\right),$$

so we can assume $k_1, k_2, k_3 \in \left[0, \pi\right]$.

The perturbation operator V is an integral operator in $L_2^o\left(\mathbb{T}^3\right)$ with the kernel

$$\left(2\pi\right)^{-\frac{3}{2}} v\left(\mathbf{q} - \mathbf{s}\right) = \left(2\pi\right)^{-\frac{3}{2}} \left(F\hat{v}\right)\left(\mathbf{q} - \mathbf{s}\right),$$

and belongs to the class of Hilbert-Schmidt operators Σ_2.

In this work, we consider the operator $H\left(\mathbf{k}\right)$ with the potential $\hat{v}$ of the form

$$\hat{v}\left(\mathbf{n}\right) = \hat{v}\left(n_1, n_2, n_3\right) = \begin{cases} \overline{v}\left(\left|\mathbf{n}\right|\right), & \left|n_1\right| + \left|n_2\right| \le 1 \\ 0, & \left|n_1\right| + \left|n_2\right| \ge 2 \end{cases} \tag{5}$$

where $\left|\mathbf{n}\right| = \left|n_1\right| + \left|n_2\right| + \left|n_3\right|$. Supporter is in the cylinder:

$$D = \left\{\mathbf{n} = \left(n_1, n_2, n_3\right) \in \mathbb{Z}^3 : n_3 \in \mathbb{Z}, \left|n_1\right| + \left|n_2\right| \le 1\right\}.$$

Since for every function $\hat{\psi} \in \ell_2^{as}\left(\left(\mathbb{Z}^3\right)^2\right)$ the equality $\hat{\psi}\left(\mathbf{x}, \mathbf{x}\right) = 0, \mathbf{x} \in \mathbb{Z}^3$ holds, then the value of the potential $\hat{v}$ at the origin can be set arbitrary, since it does not affect the result, for simplicity, we assume that $\hat{v}\left(0\right) = 0$.

The function $\overline{v}:\mathbb{N}\to\mathbb{R}$ in (5) is decreasing in $\mathbb{N}$ *i.e.*,

$$\overline{v}(1)>\overline{v}(2)>\cdots \tag{6}$$

and belongs to $\ell_2(\mathbb{N})$. The kernel v, of the integral operator V, *i.e.*, the Fourier transform $v(\mathbf{p})=(F\hat{v})(\mathbf{p})$, of the potential $\hat{v}$, has the form

$$\begin{aligned} v(\mathbf{p}) &:= (F\hat{v})(\mathbf{p}) = \frac{1}{(2\pi)^{3/2}}\sum_{\mathbf{n}\in\mathbb{Z}^3}\hat{v}(\mathbf{n})\mathrm{e}^{i(\mathbf{n},\mathbf{p})} \\ &= \frac{1}{(2\pi)^{3/2}}\Big[2\overline{v}(1)(\cos p_1+\cos p_2+\cos p_3) \\ &\quad +2\overline{v}(2)(\cos 2p_3+2\cos p_1\cos p_2+2\cos p_1\cos p_3+2\cos p_2\cos p_3) \\ &\quad +2\sum_{n=1}^{\infty}\overline{v}(n+2)\big(\cos(n+2)p_3+2\cos(n+1)p_3(\cos p_1+\cos p_2) \\ &\quad +4\cos p_1\cos p_2\cos np_3\big)\Big]. \end{aligned} \tag{7}$$

Eigenvalues of the operator $H(\mathbf{k})$. We note that the spectra of the operators $H_0(\mathbf{k})$ and V are known. The operator $H_0(\mathbf{k})$ does not have eigenvalues, its spectrum is continuous and coincides with the range of the function $\varepsilon_{\mathbf{k}}$:

$$\sigma(H_0(\mathbf{k}))=\big[m(\mathbf{k}),M(\mathbf{k})\big],\ \text{where}\ m(\mathbf{k})=\min_{\mathbf{q}\in\mathbb{T}^3}\varepsilon_{\mathbf{k}}(\mathbf{q}),\ M(\mathbf{k})=\max_{\mathbf{q}\in\mathbb{T}^3}\varepsilon_{\mathbf{k}}(\mathbf{q}).$$

The spectrum of V consists of the set $\{0,\overline{v}(n),n\in\mathbb{N}\}$. Under condition (2), the operator V is a Hilbert-Schmidt operator and is hence compact. By the Weyl theorem [10], the essential spectrum of $H(\mathbf{k})$ coincides with the spectrum of $H_0(\mathbf{k})$:

$$\sigma_{ess}(H(\mathbf{k}))=\big[m(\mathbf{k}),M(\mathbf{k})\big].$$

If $\mathbf{k}=\vec{\pi}$, then the spectrum of $H(\vec{\pi})=6I-V$ consists of eigenvalues of the form $6-\overline{v}(n),n\in\mathbb{N}$ and the essential spectrum is $\{6\}$. If $k_j=\pi$ (for some $j\in\{1,2,3\}$), then there exists a potential $\hat{v}$ such that $H(\mathbf{k})$ has an infinite number of eigenvalues outside the continuous spectrum (see [4] [14]).

We recall some notations and known facts. For any self-adjoint operator B acting in a Hilbert space $\mathscr{H}$ without an essential spectrum to the right of $\mu\in\mathbb{R}$, we let $n(\mu,B)$ denote the number of its eigenvalues to the right of μ. We let $N(\mathbf{k},z)$ denote the number of eigenvalues of $H(\mathbf{k})$ to the left of $z\le m(\mathbf{k})$, *i.e.*, $N(\mathbf{k},z)=n(-z,-H(\mathbf{k}))$. The number $N(\mathbf{k},m(\mathbf{k}))$ in fact coincides with the number of eigenvalues outside the continuous spectrum of $H(\mathbf{k})$. It follows from the self-adjointness of $H(\mathbf{k})=H_0(\mathbf{k})-V$ and positivity of V that

$$\sigma(H(\mathbf{k}))\cap(M(\mathbf{k}),\infty)=\varnothing,$$

and hence $\sigma_{disc}(H(\mathbf{k}))\subset(-\infty,m(\mathbf{k}))$. Therefore we seek only eigenvalues z less than $m(\mathbf{k})$.

For any $\mathbf{k}\in\mathbb{T}^3$ and $z<m(\mathbf{k})$, we define the integral operator

$$G(\mathbf{k},z)=V^{\frac{1}{2}}r_0(\mathbf{k},z)V^{\frac{1}{2}},$$

where $r_0(\mathbf{k},z)$ is the resolvent of the unperturbed operator $H_0(\mathbf{k})$. Under

condition (2), the operator V is positive, and we let $V^{\frac{1}{2}}$ denote the positive square root of the positive operator V. A solution f of the Schrödinger equation

$$H(\mathbf{k})f = zf$$

and the fixed points φ of $G(\mathbf{k},z)$ are connected by the relations

$$f = r_0(\mathbf{k},z)V^{\frac{1}{2}}\varphi \quad \text{and} \quad \varphi = V^{\frac{1}{2}}f.$$

The following proposition (the Birman-Schwinger principle) holds [9].

Lemma 1. *The number of eigenvalues of* $H(\mathbf{k})$ *to the left of* $z < m(\mathbf{k})$ *coincides with the number of eigenvalues of* $G(\mathbf{k},z)$ *greater than unity, i.e., the equality*

$$N(\mathbf{k},z) = n(1, G(\mathbf{k},z))$$

holds.

Lemma 2. *If for some* $\mathbf{k} \in \mathbb{T}^3$ *the limit operator* $\lim_{z\to m(\mathbf{k})-} G(\mathbf{k},z) = G(\mathbf{k},m(\mathbf{k}))$ *exists and is compact, then the equality*

$$N(\mathbf{k},m(\mathbf{k})) = n(1, G(\mathbf{k},m(\mathbf{k}))) \tag{8}$$

holds.

Equality (8) states that the number of eigenvalues of $H(\mathbf{k})$, to the left of $m(\mathbf{k})$ is equal to the number of eigenvalues of $G(\mathbf{k},m(\mathbf{k}))$ greater than unity.

3. Invariant Subspaces of $H(\mathbf{k})$

In this section, we study the invariant subspaces with respect to the operator $H(\mathbf{k})$.

Let $L_2^-(\mathbb{T}) = \{f \in L_2(\mathbb{T}) : f(-p) = -f(p)\}$ be a subspace of the space $L_2(\mathbb{T})$, consisting of odd functions on $\mathbb{T} = [-\pi,\pi]$, and $L_2^+(\mathbb{T}) = \{f \in L_2(\mathbb{T}) : f(-p) = f(p)\}$ be a subspace of $L_2(\mathbb{T})$, consisting of even functions on $\mathbb{T}$. In addition, we use the notation

$$L_{123}^-(\mathbb{T}^3) := L_2^-(\mathbb{T}) \otimes L_2^-(\mathbb{T}) \otimes L_2^-(\mathbb{T}), \quad L_{123}^+(\mathbb{T}^3) := L_2^+(\mathbb{T}) \otimes L_2^+(\mathbb{T}) \otimes L_2^+(\mathbb{T}).$$

Note that $L_{123}^-(\mathbb{T}^3)$ is a subspace of the space $L_2^o(\mathbb{T}^3)$. It is natural to expect the invariance of the subspace $L_{123}^-(\mathbb{T}^3)$ with respect to the operator $H(\mathbf{k})$. It turns out that this subspace is invariant under the operator $H(\mathbf{k})$, *i.e.* the following statement holds.

Lemma 3. *Let the potential* $\hat{v}$ *have the form* (5)*. Then the subspace* $L_{123}^-(\mathbb{T}^3)$ *is invariant under the action of* $H(\mathbf{k})$.

Proof. We prove that this subspace is invariant first with respect to $H_0(\mathbf{k})$, and then with respect to V. It follows from representation (4) that the function $\varepsilon_{\mathbf{k}}$ belongs to the subspace $L_{123}^+(\mathbb{T}^3)$, and it follows from the inclusion $f \in L_{123}^-(\mathbb{T}^3)$ that $\varepsilon_{\mathbf{k}} f \in L_{123}^-(\mathbb{T}^3)$. This proves that $L_{123}^-(\mathbb{T}^3)$ is invariant with respect to $H_0(\mathbf{k})$.

Simple calculations show that the function (see (7))

$$(Vf)(p_1,p_2,p_3)=\frac{1}{(2\pi)^{\frac{3}{2}}}\int_{\mathbb{T}^3} v(p_1-s_1,p_2-s_2,p_3-s_3)\,f(s_1,s_2,s_3)\mathrm{d}s_1\mathrm{d}s_2\mathrm{d}s_3$$

belongs to the subspace $L_{123}^-(\mathbb{T}^3)$ for $f\in L_{123}^-(\mathbb{T}^3)$. Hence, we prove the invariance of $L_{123}^-(\mathbb{T}^3)$ with respect to V, and it follows that $L_{123}^-(\mathbb{T}^3)$ is invariant with respect to $H(\mathbf{k})=H_0(\mathbf{k})-V$.

$H_{123}^-(\mathbf{k})$ denotes the restriction of $H(\mathbf{k})$ to the respective subspace $L_{123}^-(\mathbb{T}^3)$. The action of $H_{0(123)}^-(\mathbf{k}):=H_0(\mathbf{k})$ is unchanged, the unperturbed operator $H_0(\mathbf{k})$ is an operator of multiplication by the function $\varepsilon_{\mathbf{k}}$. We present the formula for $V_{123}^-=V\big|_{L_{123}^-(\mathbb{T}^3)}$ operator V acts on the element $f\in L_{123}^-(\mathbb{T}^3)$ according to the formula

$$\left(V_{123}^-f\right)(\mathbf{p})=\frac{1}{\pi^3}\sum_{n=1}^{\infty}\overline{v}(n+2)\int_{\mathbb{T}^3}\sin p_1\sin p_2\sin np_3\sin q_1\sin q_2\sin nq_3\,f(\mathbf{q})\mathrm{d}\mathbf{q}.$$

Note that for $\mathbf{k}=\vec{\pi}$, the spectrum of $H(\vec{\pi})=6I-V$ consists only of the eigenvalues $6,6-\overline{v}(n),n\in\mathbb{N}$ and the essential spectrum $\{6\}$. Under condition (6) the number $z_1(\vec{\pi})=6-\overline{v}(1)$ is a threefold eigenvalue of $H(\vec{\pi})$, with the corresponding eigenfunctions

$$\sin p_1,\sin p_2,\sin p_3,$$

the number $z_2(\vec{\pi})=6-\overline{v}(2)$ is a sevenfold eigenvalue with the corresponding eigenfunctions

$$\sin 2p_3,\cos p_1\sin p_2,\sin p_1\cos p_2,\cos p_1\sin p_3,$$
$$\sin p_1\cos p_3,\cos p_2\sin p_3,\sin p_2\cos p_3,$$

for each $n\geq 3$, the number $z_n(\vec{\pi})=6-\overline{v}(n)$ is a ninefold eigenvalue, and the corresponding eigenfunctions are

$$\sin(n+2)p_3,\sin p_1\cos(n+1)p_3,\sin p_2\cos(n+1)p_3,$$
$$\sin(n+1)p_3\cos p_1,\sin(n+1)p_3\cos p_2,\sin np_3\cos p_1\cos p_2,$$
$$\sin p_2\cos p_1\cos np_3,\sin p_1\cos p_2\cos np_3,\sin p_1\sin p_2\sin np_3.$$

The number $z_\infty(\vec{\pi})=6$ is an eigenvalue of an infinite multiplicity, and the corresponding eigenfunctions are

$$\psi_{(n_1,n_2,n_3)}^{---}(\mathbf{p})=\sin n_1p_1\sin n_2p_2\sin n_3p_3,\ \ n_3\in\mathbb{N},\ n_1+n_2\geq 3.$$

All ninefold eigenvalues $z_n(\vec{\pi})=6-\overline{v}(n),n\geq 3$ of the operator $H(\vec{\pi})$ are simple eigenvalues for the operator $H_{123}^-(\vec{\pi})$, and the number $z_\infty(\vec{\pi})=6$ is an eigenvalue of an infinite multiplicity.

If the third coordinate k_3 of the total quasimomentum $\mathbf{k}$ is equal to π, then the operator $H(k_1,k_2,\pi)$ has infinitely many invariant subspaces $\mathfrak{R}_{123}^-(n),n\in\mathbb{N}$.

Next, we give a description of the invariant subspace $\mathfrak{R}_{123}^-(n),n\in\mathbb{N}$.

The system of functions

$$\left\{\psi_n^-(q)=\frac{1}{\sqrt{\pi}}\sin nq\right\}_{n\in\mathbb{N}}$$

is an orthonormal basis in the space $L_2^-(\mathbb{T})$. Let us denote by $L^-(n), n\in\mathbb{N}$ the one-dimensional subspace spanned by the vector ψ_n^-. The space $L_2^-(\mathbb{T})$ can be decomposed into the direct sum

$$L_2^-(\mathbb{T})=\sum_{n=1}^{\infty}\oplus L^-(n).$$

This decomposition produces another decomposition

$$\begin{aligned}L_{123}^-(\mathbb{T}^3)&=\sum_{n=1}^{\infty}\oplus\left\{L_2^-(\mathbb{T})\otimes L_2^-(\mathbb{T})\otimes L^-(n)\right\}\\&=\sum_{n=1}^{\infty}\oplus\left\{L_{12}^-(\mathbb{T}^2)\otimes L^-(n)\right\}=\sum_{n=1}^{\infty}\oplus\mathfrak{R}_{123}^-(n),\end{aligned}$$

where

$$\mathfrak{R}_{123}^-(n):=L_{12}^-(\mathbb{T}^2)\otimes L^-(n),\quad L_{12}^-(\mathbb{T}^2)=L_2^-(\mathbb{T})\otimes L_2^-(\mathbb{T}).$$

Lemma 4. *Let the potential* $\hat{v}$ *have the form* (5). *Then the subspace* $\mathfrak{R}_{123}^-(n)$ *is invariant under* $H_{123}^-(k_1,k_2,\pi)$ for any $n\in\mathbb{N}$.

Proof. Let $\left(f\psi_n^-\right)(p_1,p_2,p_3):=f(p_1,p_2)\psi_n^-(p_3)$, where $f\in L_{12}^-(\mathbb{T}^2)$, $\psi_n^-\in L^-(n)$ is an arbitrary element of $\mathfrak{R}_{123}^-(n)$. We consider the action of $H_{123}^-(k_1,k_2,\pi)=H_0(k_1,k_2,\pi)-V_{123}^-$ on $f\psi_n^-$:

$$\begin{aligned}&\left(H_0(k_1,k_2,\pi)f\psi_n^-\right)(\mathbf{p})\\&=\left[\left(6-2\cos\frac{k_1}{2}\cos p_1-2\cos\frac{k_2}{2}\cos p_2\right)f(p_1,p_2)\right]\psi_n^-(p_3),\end{aligned}\tag{9}$$

$$\begin{aligned}&\left(V_{123}^-f\psi_n^-\right)(\mathbf{p})\\&=\left[\frac{\overline{v}(n+2)}{\pi^2}\int_{\mathbb{T}^2}\sin p_1\sin q_1\sin p_2\sin q_2 f(q_1,q_2)\mathrm{d}q_1\mathrm{d}q_2\right]\psi_n^-(p_3).\end{aligned}\tag{10}$$

To obtain the last formula (10), we use the orthogonality of the system of functions $\left\{\psi_n^-\right\}_{n\in\mathbb{N}}$ in $L_2^-(\mathbb{T})$. Relations (9) and (10) imply the equality

$$\begin{aligned}&\left(H_{123}^-(k_1,k_2,\pi)f\psi_n^-\right)(p_1,p_2,p_3)\\&=\left(H_0(k_1,k_2,\pi)f\psi_n^-\right)(p_1,p_2,p_3)-\left(V_{123}^-f\psi_n^-\right)(p_1,p_2,p_3)\\&=\left[\left(6-2\cos\frac{k_1}{2}\cos p_1-2\cos\frac{k_2}{2}\cos p_2\right)f(p_1,p_2)\right]\psi_n^-(p_3)\\&\quad-\left[\frac{\overline{v}(n+2)}{\pi^2}\int_{\mathbb{T}^2}\sin p_1\sin q_1\sin p_2\sin q_2 f(q_1,q_2)\mathrm{d}q_1\mathrm{d}q_2\right]\psi_n^-(p_3)\end{aligned}\tag{11}$$

which completes the proof of the lemma.

We denote by $H_{123n}^-(k_1,k_2,\pi)$ restriction of the operator $H_{123}^-(k_1,k_2,\pi)$ in the invariant subspace $\mathfrak{R}_{123}^-(n)$. Formula (11) shows that the restriction $H_{123n}^-(k_1,k_2,\pi)$ to the subspace $\mathfrak{R}_{123}^-(n)=L_{12}^-(\mathbb{T}^2)\otimes L^-(n)$ has the form

$$H_{123n}^-(k_1,k_2,\pi)=\left[2I+H_0(k_1,k_2)-\overline{v}(n+2)V_{11}\right]\otimes I,\tag{12}$$

where I is the identity operator and $H_{123}^{(n)}(\mathbf{k}):=2I+H_0(\mathbf{k})-\overline{v}(n+2)V_{11}$, $\mathbf{k}=(k_1,k_2)$, is a two-dimensional two-particle operator acting in $L_{12}^-(\mathbb{T}^2)$ by

the formula

$$\left(H_{123}^{(n)}(\mathbf{k})f\right)(\mathbf{p})$$
$$=\left(2+\varepsilon_{\mathbf{k}}(\mathbf{p})\right)f(\mathbf{p})-\frac{\overline{v}(n+2)}{\pi^2}\int_{\mathbb{T}^2}\sin p_1\sin p_2\sin q_1\sin q_2 f(\mathbf{q})\mathrm{d}\mathbf{q},$$

where $\varepsilon_{\mathbf{k}}(\mathbf{p})=4-2\cos\frac{k_1}{2}\cos p_1-2\cos\frac{k_2}{2}\cos p_2$, and V_{11} is a one-dimensional integral operator in $L_{12}^{-}(\mathbb{T}^2)$ with the kernel

$$v(\mathbf{p},\mathbf{q})=\frac{1}{\pi^2}\sin p_1\sin p_2\sin q_1\sin q_2.$$

Studying the eigenvalues of $H_{123n}^{-}(k_1,k_2,\pi)$ by representations (12) reduces to studying the eigenvalues of

$$H_{123}^{(n)}(\mathbf{k})=2I+H_0(\mathbf{k})-\overline{v}(n+2)V_{11},\mathbf{k}=(k_1,k_2)$$

i.e. the three-dimensional problem reduces to the two-dimensional problem.

4. Eigenvalues of the Operator $H_{123}^{-}(\mathbf{k})$

Our main goal in this section is to study the behavior of the nondegenerate eigenvalue $z_{n+2}(\vec{\pi})=6-\overline{v}(n+2), n\in\mathbb{N}$ of $H_{123}^{-}(\vec{\pi})$ at small perturbations β ($k_1=\pi-2\beta$ or $k_2=\pi-2\beta$), *i.e.* the eigenvalues of $H_{123}^{-}(\pi-2\beta,\pi,\pi)$ (or $H_{123}^{-}(\pi,\pi-2\beta,\pi)$) at small perturbations β. The studying of the eigenvalues of $H_{123}^{-}(\pi-2\beta,\pi,\pi)$ is reduced to study the eigenvalues of the operator $H_{123n}^{-}(\pi-2\beta,\pi,\pi)$ for each fixed $n\in\mathbb{N}$. In turn, the problem of studying the eigenvalues of the operator $H_{123n}^{-}(\pi-2\beta,\pi,\pi)$ by virtue of (12) is reduced to study of the discrete spectrum of the operator

$$H_{123}^{(n)}(\pi-2\beta,\pi)=2I+H_0(\pi-2\beta,\pi)-\overline{v}(n+2)V_{11}.$$

Studying the eigenvalues of $H_{123}^{(n)}(\pi-2\beta,\pi)$ and $H_{123}^{(n)}(\pi,\pi-2\beta)$ reduces to studying the eigenvalues of $H_\lambda(k)$ acting in $L_2^{-}(\mathbb{T})$ by the formula

$$\begin{aligned}&\left(H_\lambda(k)f\right)(p)=\varepsilon_k(p)f(p)-\frac{\lambda}{\pi}\int_{\mathbb{T}}\sin p\sin q f(q)\mathrm{d}q,\\&\varepsilon_k(p)=2-2\cos\frac{k}{2}\cos p.\end{aligned}\tag{13}$$

It is known that the essential spectrum of $H_\lambda(\pi-2\beta)=H_0(\pi-2\beta)-\lambda V_1, \beta\in\left(0,\frac{\pi}{2}\right]$ consists of a segment $\left[m(\beta),M(\beta)\right]$, where $m(\beta)=2-2\sin\beta$, $M(\beta)=2+2\sin\beta$.

Further we give some information about the eigenvalues and eigenfunctions of the operator $H_\lambda(k)$. Combining Theorem 6.3 in [6], Theorem 5.10 in [15] and Lemmas 1 and 2 we obtain the following statement about eigenvalues of the operator $H_\lambda(k)$.

Lemma 5. *Let* $\beta\in\left(0,\frac{\pi}{2}\right]$.

a) If $\lambda < \sin\beta$, then the operator $H_\lambda(\pi - 2\beta)$ has no eigenvalues lying outside of the essential spectrum.

b) If $\lambda = \sin\beta$, then the left edge $m(\beta)$ of essential spectrum of the operator $H_\lambda(\pi - 2\beta)$ is a resonance.

c) If $\lambda > \sin\beta$, then the operator $H_\lambda(\pi - 2\beta)$ has a unique nondegenerate eigenvalue

$$z_\lambda(\beta) = 2 - \lambda - \frac{1}{\lambda}\sin^2\beta$$

which lying in the left of the essential spectrum with corresponding normalized eigenfunction

$$f_\lambda^-(p) = \frac{C_\lambda \sin p}{2 - 2\sin\beta\cos p - z_\lambda(\beta)} \in L_2^-(\mathbb{T}). \tag{14}$$

Here C_λ is the normalizing multiplicity.

d) The operator $H_\lambda(\pi - 2\beta)$ has no embedded eigenvalues in the interval $(m(\beta), M(\beta))$.

Hilbert space $L_{12}^-(\mathbb{T}^2) = L_2^-(\mathbb{T}) \otimes L_2^-(\mathbb{T})$ can be written as a direct sum:

$$L_2^-(\mathbb{T}) \otimes L_2^-(\mathbb{T}) = L_2^-(\mathbb{T}) \otimes L^-(1) \oplus \left(L_2^-(\mathbb{T}) \otimes L^-(1)\right)^\perp.$$

The following lemma establishes a connection between the operators $H_{123}^{(n)}(\pi - 2\beta, \pi)$ and $H_\lambda(k)$.

Lemma 6. *Let the potential* $\hat{v}$ *have the form* (5). *Then:*

a) the subspace $L_2^-(\mathbb{T}) \otimes L^-(1)$ and its orthogonal complement $\left(L_2^-(\mathbb{T}) \otimes L^-(1)\right)^\perp$ are invariant under $H_{123}^{(n)}(\pi - 2\beta, \pi)$.

b) restriction of the operator $H_{123}^{(n)}(\pi - 2\beta, \pi)$ to the invariant subspace $\left(L_2^-(\mathbb{T}) \otimes L^-(1)\right)^\perp$ coinsides with the unperturbed operator $H_0(\pi - 2\beta, \pi)$.

c) restriction of the operator $H_{123}^{(n)}(\pi - 2\beta, \pi)$ to the invariant subspace $L_2^-(\mathbb{T}) \otimes L^-(1)$ can be represented as a tensor product:

$$H_{123}^{(n)}(\pi - 2\beta, \pi) = \left[4I + H_0(\pi - 2\beta) - \overline{v}(n+2)V_1\right] \otimes I. \tag{15}$$

Here, I is the identity operator, and $H_{\lambda(n)}(\pi - 2\beta) := H_0(\pi - 2\beta) - \lambda(n)V_1$, $\lambda(n) = \overline{v}(n+2)$ is a one-dimensional two-particle operator acting in $L_2^-(\mathbb{T})$ by the formula (13).

This lemma is proved in the same way as the Lemma 4. In particular, part b) of the lemma implies that the operator $H_{123}^{(n)}(\pi - 2\beta, \pi)$ has no eigenfunctions in $\left(L_2^-(\mathbb{T}) \otimes L^-(1)\right)^\perp$. Thus, studying the eigenvalues of the operator $H_{123}^{(n)}(\pi - 2\beta, \pi)$ is reduced to studying eigenvalues of the operator $H_{\lambda(n)}(\pi - 2\beta) = H_0(\pi - 2\beta) - \lambda(n)V_1$.

From Lemmas 5 - 6 and tensor product (15) implies the following statement regarding operator $H_{123}^{(n)}(\pi - 2\beta, \pi)$.

Theorem 1. *Let* $\beta \in \left(0, \frac{\pi}{2}\right]$ *and* $n \in \mathbb{N}$.

a) If $\overline{v}(n+2) < \sin\beta$, then the operator $H_{123}^{(n)}(\pi - 2\beta, \pi)$ has no eigenvalues lying outside of the essential spectrum.

b) If $\overline{\nu}(n+2)=\sin\beta$, then the left edge $m(\beta)$ of essential spectrum of the operator $H_{123}^{(n)}(\pi-2\beta,\pi)$ is a resonance.

c) If $\overline{\nu}(n+2)>\sin\beta$, then the operator $H_{123}^{(n)}(\pi-2\beta,\pi)$ has a unique non-degenerate eigenvalue

$$z_{123}^{(n)}(\pi-2\beta,\pi)=4+z_{\lambda(n)}(\beta)=6-\overline{\nu}(n+2)-\frac{1}{\overline{\nu}(n+2)}\sin^2\beta, \tag{16}$$

which lies in the left of the essential spectrum and with the corresponding normalized eigenfunction

$$f_{\lambda(n)}^{--}(p_1,p_2)=f_{\lambda(n)}^{-}(p_1)\frac{\sin p_2}{\sqrt{\pi}}=f_{\lambda(n)}^{-}(p_1)\psi_1^{-}(p_2)\in L_2^{-}(\mathbb{T})\otimes L^{-}(1),$$

where $f_{\lambda(n)}^{-}$ is the normalized eigenfunction of the operator $H_{\lambda(n)}(\pi-2\beta)$ corresponding to the eigenvalue $z_{\lambda(n)}(\beta)$, the operator $H_{\lambda(n)}(k)$ is defined by the formula (13).

d) The operator $H_{123}^{(n)}(\pi-2\beta,\pi)$ has no embedded eigenvalues in the interval $(m(\beta),M(\beta))$.

Similar statement is true for the operator $H_{123}^{(n)}(\pi,\pi-2\beta)$. The eigenvalues of the operators $H_{123}^{(n)}(\pi,\pi-2\beta)$ and $H_{123}^{(n)}(\pi-2\beta,\pi)$ are same, but eigenfunctions differ with variable replacement p_1 and p_2. In other words, the operators $H_{123}^{(n)}(k_1,k_2)$ and $H_{123}^{(n)}(k_2,k_1)$ are unitary equivalent. Therefore, the operators $H_{123n}^{-}(k_1,k_2,\pi)$ and $H_{123n}^{-}(k_2,k_1,\pi)$ are unitary equivalent too.

Similar statement can relatively be formulated for the operator $H_{123}^{(n)}(\pi-2\beta,\pi-2\beta)$. For this purpose, we introduce the following notation. Through

$$\Delta_n(\beta,z)=1-\frac{\overline{\nu}(n+2)}{\pi^2}\int_{\mathbb{T}^2}\frac{\sin^2 p_1\sin^2 p_2\,\mathrm{d}p_1\mathrm{d}p_2}{2+2(2-\sin\beta\cos p_1-\sin\beta\cos p_2)-z}$$

we denote the Fredholm determinant of the operator $I-\overline{\nu}(n+2)V_{11}r_0(\beta,z)$, where $r_0(\beta,z)$ is the resolvent of the operator $2I+H_0(\pi-2\beta,\pi-2\beta)$, and V_{11} is an integral operator with the kernel

$$v(\mathbf{p},\mathbf{q})=\frac{1}{\pi^2}\sin p_1\sin p_2\sin q_1\sin q_2.$$

Through C_{11}^{--} denote the value of the following integral:

$$C_{11}^{--}=\frac{1}{\pi^2}\int_{\mathbb{T}^2}\frac{\sin^2 p_1\sin^2 p_2\,\mathrm{d}p_1\mathrm{d}p_2}{2(2-\cos p_1-\cos p_2)}=\int_{\mathbb{T}^2}\frac{\left|\psi_1^{-}(p_1)\right|^2\left|\psi_1^{-}(p_2)\right|^2\mathrm{d}p_1\mathrm{d}p_2}{2\varepsilon(\mathbf{p})}.$$

Simple calculations reveal the following approximate value $C_{11}^{--}\approx 0.302347$.

Theorem 2. *Let* $\beta\in\left(0,\frac{\pi}{2}\right]$, $n\in\mathbb{N}$.

a) If $\overline{\nu}(n+2)<\frac{\sin\beta}{C_{11}^{--}}$, then the operator $H_{123}^{(n)}(\pi-2\beta,\pi-2\beta)$ has no eigenvalues lying outside of the essential spectrum.

b) If $\overline{\nu}(n+2)=\frac{\sin\beta}{C_{11}^{--}}$, then the left edge $m(\beta)=6-4\sin\beta$ of the spectrum

of the operator $H_{123}^{(n)}(\pi-2\beta,\pi-2\beta)$ is an eigenvalue.

c) If $\overline{v}(n+2)>\dfrac{\sin\beta}{C_{11}^{--}}$, then the operator $H_{123}^{(n)}(\pi-2\beta,\pi-2\beta)$ has a unique nondegenerate eigenvalue $z_{123}^{(n)}(\pi-2\beta,\pi-2\beta)$ below the essential spectrum.

d) The operator $H_{123}^{(n)}(\pi-2\beta,\pi-2\beta)$ has no embedded eigenvalues in the interval $(m(\beta),M(\beta))$.

This theorem is proved in similar way as Lemma 5. There are some differences:

1) In the Theorem 2, the eigenvalue $z_{123}^{(n)}(\pi-2\beta,\pi-2\beta)$ was calculated with the accuracy of β^2:

$$z_{123}^{(n)}(\pi-2\beta,\pi-2\beta)=6-\overline{v}(n+2)-\frac{2}{\overline{v}(n+2)}\sin^2\beta+O(\beta^4)$$

and corresponding normalized eigenfunction has the form

$$f_{123}^{(n)}(p_1,p_2)=\frac{C_n(\beta)\sin p_1\sin p_2}{6-2\sin\beta\cos p_1-2\sin\beta\cos p_2-z_{123}^{(n)}(\pi-2\beta,\pi-2\beta)}\in L_{12}^{-}(\mathbb{T}^2),\tag{17}$$

where $C_n(\beta)$ is the normalizing multiplicity.

2) Left edge $m(\beta)=6-2\sin\beta$ of the essential spectrum is a resonance for the operator $H_{123}^{(n)}(\pi-2\beta,\pi)$, but for the operator $H_{123}^{(n)}(\pi-2\beta,\pi-2\beta)$ the left edge $m(\beta)=6-4\sin\beta$ of the essential spectrum is the eigenvalue, *i.e.* the equation $H_{123}^{(n)}(\pi-2\beta,\pi-2\beta)f=m(\beta)f$ has a non-trivial solution

$$f(p_1,p_2)=\frac{C\sin p_1\sin p_2}{2-\cos p_1-\cos p_2}$$

and it belongs to $L_{12}^{-}(\mathbb{T}^2)$.

5. Conclusions

1) We have shown that the operator $H_{123}^{-}(k_1,k_2,\pi)$ has infinitely many invariant subspaces $\mathfrak{R}_{123}^{-}(n), n\in\mathbb{N}$. It has been proved that if condition $\overline{v}(n+2)>\sin\beta$ holds then the operator $H_{123n}^{-}(\pi-2\beta,\pi,\pi)$ has a unique simple eigenvalue $z_{123}^{(n)}(\pi-2\beta,\pi)$ of the form (16), otherwise, the operator has no eigenvalues outside of the essential spectrum. A similar statement holds for the operator $H_{123n}^{-}(\pi-2\beta,\pi-2\beta,\pi)$.

2) Without loss of generality it can be assumed that $\overline{v}(3)\le 1$. Since, if $\overline{v}(3)>1$ then it follows from $\lim_{n\to\infty}\overline{v}(n)=0$ that there exists a number $m\in\mathbb{N}$ such that $\overline{v}(m+2)\le 1$ and monotonicity of $\overline{v}$ implies that $\overline{v}(n)>1$ for $n=3,4,\cdots,m+1$, and in this case, the eigenvalues $z_{123}^{(n)}(\pi-2\beta,\pi), n=1,2,\cdots,m-1$ of $H_{123}^{-}(\pi-2\beta,\pi,\pi)$ exist for all $\beta\in[0,\pi/2]$.

For a fixed $\beta\in(0,\pi/2]$ there exists $m\in\mathbb{N}$ such that $\sin\beta\in(\overline{v}(m+3),\overline{v}(m+2))$ and the operator $H_{123}^{-}(\pi-2\beta,\pi,\pi)$ has m non-degenerate eigenvalues outside of the essential spectrum (see Theorem 1):

$$z_{123}^{(1)}(\pi-2\beta,\pi,\pi):=z_{123}^{(1)}(\pi-2\beta,\pi)=6-\overline{\nu}(3)-\frac{1}{\overline{\nu}(3)}\sin^2\beta,$$

$$z_{123}^{(2)}(\pi-2\beta,\pi,\pi):=z_{123}^{(2)}(\pi-2\beta,\pi)=6-\overline{\nu}(4)-\frac{1}{\overline{\nu}(4)}\sin^2\beta,$$

$$\vdots$$

$$z_{123}^{(m)}(\pi-2\beta,\pi,\pi):=z_{123}^{(m)}(\pi-2\beta,\pi)=6-\overline{\nu}(m+2)-\frac{1}{\overline{\nu}(m+2)}\sin^2\beta.$$

The corresponding normalized eigenfunctions are of the forms:

$$f_{123\lambda(1)}^{---}(p_1,p_2,p_3)=f_{\lambda(1)}^{-}(p_1)\psi_1^{-}(p_2)\psi_1^{-}(p_3)\in L_2^{-}(\mathbb{T})\otimes L^{-}(1)\otimes L^{-}(1),$$

$$f_{123\lambda(2)}^{---}(p_1,p_2,p_3)=f_{\lambda(2)}^{-}(p_1)\psi_1^{-}(p_2)\psi_2^{-}(p_3)\in L_2^{-}(\mathbb{T})\otimes L^{-}(1)\otimes L^{-}(2),$$

$$\vdots$$

$$f_{123\lambda(m)}^{---}(p_1,p_2,p_3)=f_{\lambda(m)}^{-}(p_1)\psi_1^{-}(p_2)\psi_m^{-}(p_3)\in L_2^{-}(\mathbb{T})\otimes L^{-}(1)\otimes L^{-}(m),$$

where, $f_{\lambda(m)}^{-}$ is the normalized eigenfunction of the operator $H_{\lambda(m)}(\pi-2\beta)$ corresponding to the eigenvalue $z_{\lambda(m)}(\beta)$ and the operator $H_{\lambda(m)}(k)$ is defined by the formula (13), $\lambda(m)=\overline{\nu}(m+2)$.

The eigenvalues of the operators $H_{123}^{-}(\pi-2\beta,\pi,\pi)$ and $H_{123}^{-}(\pi,\pi-2\beta,\pi)$ are same but eigenfunctions differ with variable replacement p_1 and p_2. In other words, the operators $H_{123}^{-}(\pi-2\beta,\pi,\pi)$ and $H_{123}^{-}(\pi,\pi-2\beta,\pi)$ are unitary equivalent.

In the case $\sin\beta=\overline{\nu}(m+2)$, the left edge $m(\beta)=6-2\sin\beta$ of the essential spectrum is a resonance of the operator $H_{123}^{-}(\pi-2\beta,\pi,\pi)$ (see Theorem 1).

3) Let for some $m\in\mathbb{N}$ the relation $\sin\beta\in\left(\overline{\nu}(m+3)C_{11}^{--},\overline{\nu}(m+2)C_{11}^{--}\right)$ hold then the operator $H_{123}^{-}(\pi-2\beta,\pi-2\beta,\pi)$ has m nondegenerate eigenvalues outside the essential spectrum (see Theorem 2) and for small β:

$$z_{123}^{(1)}(\pi-2\beta,\pi-2\beta,\pi):=z_{123}^{(1)}(\pi-2\beta,\pi-2\beta)$$
$$=6-\overline{\nu}(3)-\frac{2}{\overline{\nu}(3)}\sin^2\beta+O(\beta^4),$$

$$z_{123}^{(2)}(\pi-2\beta,\pi-2\beta,\pi):=z_{123}^{(2)}(\pi-2\beta,\pi-2\beta)$$
$$=6-\overline{\nu}(4)-\frac{2}{\overline{\nu}(4)}\sin^2\beta+O(\beta^4),$$

$$\vdots$$

$$z_{123}^{(m)}(\pi-2\beta,\pi-2\beta,\pi):=z_{123}^{(m)}(\pi-2\beta,\pi-2\beta)$$
$$=6-\overline{\nu}(m+2)-\frac{2}{\overline{\nu}(m+2)}\sin^2\beta+O(\beta^4).$$

The corresponding normalized eigenfunctions are of the forms:

$$f_{123}^{(1)-}(p_1,p_2,p_3)=f_{123}^{(1)}(p_1,p_2)\psi_1^{-}(p_3)\in L_{12}^{-}(\mathbb{T}^2)\otimes L^{-}(1),$$

$$f_{123}^{(2)-}(p_1,p_2,p_3)=f_{123}^{(2)}(p_1,p_2)\psi_2^{-}(p_3)\in L_{12}^{-}(\mathbb{T}^2)\otimes L^{-}(2),$$

$$\vdots$$

$$f_{123}^{(m)-}(p_1,p_2,p_3)=f_{123}^{(m)}(p_1,p_2)\psi_m^-(p_3)\in L_{12}^-\left(\mathbb{T}^2\right)\otimes L^-(m),$$

where, $f_{123}^{(m)}$ is the normalized eigenfunction of the operator $H_{123}^{(m)}(\pi-2\beta,\pi-2\beta)$ corresponding to the eigenvalue $z_{123}^{(m)}(\pi-2\beta,\pi-2\beta)$ defined by the formula (17).

In the case $\sin\beta=\overline{v}(m+2)C_{11}^{--}$, the left edge $m(\beta)=6-4\sin\beta$ of the essential spectrum is the eigenvalue of $H_{123}^-(\pi-2\beta,\pi-2\beta,\pi)$ (see Theorem 2) with the corresponding eigenfunction

$$f(\mathbf{p})=\frac{C\sin p_1\sin p_2}{2-\cos p_1-\cos p_2}\cdot\sin mp_3\in L_{12}^-\left(\mathbb{T}^2\right)\otimes L^-(m).$$

Remark 1. If the potential $\hat{v}$ is even in all arguments p_1,p_2,p_3 and the condition $\hat{v}\in\ell_2\left(\mathbb{Z}^3\right)$ holds, then the statements of Lemmas 3 - 4 remain valid.

Remark 2. If $k_3\neq\pi$, then the subspaces $\mathfrak{R}_{123}^-(n),n\in\mathbb{N}$ are not invariant under the operator $H_{123}^-(k_1,k_2,k_3)$.

Acknowledgements

This work was supported by the Grant OT-F4-66 of Fundamental Science Foundation of Uzbekistan.

Conflicts of Interest

The authors declare no conflicts of interest regarding the publication of this paper.

References

[1] Mamatov, Sh.S. and Minlos, R.A. (1989) *Theoretical and Mathematical Physics*, **79**, 455-466. https://doi.org/10.1007/BF01016525

[2] Minlos, R.A. and Mogilner, A.I. (1989) Some Problems Concerning Spectra of Lattice Models. In: Exner, P. and Seba, P., Eds., *Schrödinger Operators*: *Standard and Nonstandard*, World. Scientific, Singapore, 243-257.

[3] Howland, J.S. (1974) *Pacific Journal of Mathematics*, **55**, 157-176. https://doi.org/10.2140/pjm.1974.55.157

[4] Abdullaev, J.I. (2006) *Theoretical and Mathematical Physics*, **147**, 486-495. https://doi.org/10.1007/s11232-006-0055-z

[5] Rauch, J. (1980) *Journal of Functional Analysis*, **35**, 304-315. https://doi.org/10.1016/0022-1236(80)90085-3

[6] Abdullaev, J.I. and Kuliev, K.D. (2016) *Theoretical and Mathematical Physics*, **186**, 231-250. https://doi.org/10.1134/S0040577916020082

[7] Muminov, M.I. and Ghoshal, S.K. (2020) *Complex Analysis and Operator Theory*, **14**, Article No. 11. https://doi.org/10.1007/s11785-019-00978-z

[8] Abdullaev, J.I. (2005) *Theoretical and Mathematical Physics*, **145**, 1551-1558. https://doi.org/10.1007/s11232-005-0182-y

[9] Abdullaev, J.I. and Ikromov, I.A. (2007) *Theoretical and Mathematical Physics*, **152**, 1299-1312. https://doi.org/10.1007/s11232-007-0114-0

[10] Reed, M. and Simon, B. (1978) Methods of Modern Mathematical Physics Ser.: Analysis of Operators.

[11] Simon, B. (1976) *Annals of Physics*, **97**, 279-288. https://doi.org/10.1016/0003-4916(76)90038-5

[12] Klaus, M. (1977) *Annals of Physics*, **108**, 288-300. https://doi.org/10.1016/0003-4916(77)90015-X

[13] Faria da Viega, P.A., Ioriatti, L. and O'Carrol, M. (2002) *Physical Review E*, **66**, Article ID: 016130. https://doi.org/10.1103/PhysRevE.66.016130

[14] Abdullaev, J.I. (2005) *Uzbek Mathematical Journal*, No. 1, 3-11.

[15] Ando, K., Isozaki, H. and Morioka, H. (2016) *Annales Henri Poincaré*, **17**, 2103-2171. https://doi.org/10.1007/s00023-015-0430-0

Journal of Modern Physics, 2021, 12, 50-58
https://www.scirp.org/journal/jmp
ISSN Online: 2153-120X
ISSN Print: 2153-1196

A Physical Origin for Quantum Entanglement and Probabilistic Behaviors

Kenneth H. Schatten[1,2]

[1]NASA/GSFC, Greenbelt, MD, USA
[2]Now at Ai-Solutions, Inc. Lanham, MD, USA
Email: kschatten@alum.mit.edu

How to cite this paper: Schatten, K.H. (2021) A Physical Origin for Quantum Entanglement and Probabilistic Behaviors. *Journal of Modern Physics*, **12**, 50-58.
https://doi.org/10.4236/jmp.2021.121005

Received: August 7, 2020
Accepted: January 11, 2021
Published: January 14, 2021

Abstract

Quantum Mechanics' entanglement and probabilistic behaviors are viewed in the light of Quantum Field Theory's (QFT's) advances made during the last century. In particular, Bohm's version (B-EPR) of the Einstein, Podolsky, Rosen (EPR) experiment is now viewed with the aid of QFT's modern description of electrons. In QFT, free electrons possess a bare core surrounded by a "dressing". The dressing consists of one or more virtual particles/fields pulled from the vacuum during the bound electron's parturition. In QFT, a bound electron's freedom is aided by eliminating its energy losses from bremsstrahlung. The paper develops a "Shimony" numerical model using QFT's free electron structure with the aid of a "random vector paradigm" (RVP). The RVP simply expresses QFT's free electron as a bare core surrounded by an EM dressing. Using this RVP, we imbue newly freed electrons with a vector-like EM spin property of 1/2. From this, the Shimony Monte Carlo computer analysis provides a detailed comparison of the B-EPR experiment as described by Bell. The entanglement property can serve to provide a way to transport shared encoded information. Overall, the electron dressing can convey random elements that may provide QM with its entanglement and probabilistic behaviors.

Keywords

Quantum Mechanics, Entanglement, Probability, Einstein, Electron, Origin, Structure

1. Introduction

The background of this research harkens back to the origins of Quantum Mechanics (QM) early in the 20th century. QM's entanglement and probabilistic attributes arose then, and scientists were puzzled by its meaning and behaviors. These views were finalized in a meeting of top QM physicists, using the term:

"The Copenhagen Interpretation", with the probabilistic aspect meant to describe the quantum wave function, ψ, as being a measure of probability, as opposed to a "real" physical property, such as mass density or charge density. Several of the world's best physical theorists at the time, such as Einstein and Schrodinger, objected to this, as probabilities are usually associated with random events, requiring a source of a random element, such as the use of cards or dice. Thus it was upon hearing of this interpretation, Einstein was reported to have declared "God does not play dice with the Universe". Neils Bohr, the founder of the probabilistic interpretation, said: "Einstein, stop telling God what to do". QM also required the existence of another strange phenomenon, called "entanglement". As a result of the Copenhagen meeting, the theoretical viewpoint moved towards the current probabilistic and entanglement viewpoints with a dearth of physical understanding as to why QM exhibits these novel mannerisms.

This paper explores the origin of Quantum Mechanics' 1) behaviors of entanglement, 2) probabilistic as well as, at times yielding a 3) 100% deterministic response, which may simply be regarded as a probabilistic process of ±1, with negative values indicating probabilities of oppositely oriented spin. These behaviors are displayed through a Monte Carlo computer analysis of the role of electron structure as this affects these three properties. It behooves us to understand how elementary particles may acquire, possess and display these three QM behaviors. To answer this, we need to find a way that seemingly identical electrons can behave individualistically. Namely, consider two electrons: A and B; these two can result in electron A doing one thing and electron B doing another. Hence, seemingly identical electrons need to have specific properties that allow each individual particle to behave individually in accordance with the above three unique attributes. Thus QM displays a puzzling mixture of deterministic, probabilistic and entanglement behaviors.

On the subject of random behaviors, the kinetic theory of gases does have molecules appearing to behave randomly, similar to a stochastic behavior; however, quantum effects are associated with quantization and interference effects totally unlike molecular stochastic behavior. The latter can be understood owing to the huge number of individual molecules involved. Their motions can also be viewed very much as billiard balls classically colliding with one another. The responses are simply associated with the momentum changes and transferring momentum and energy. So, there is a world of difference between classical effects compared with quantum mechanics' digitization associated with its unique discrete quantum jumps plus the plethora of other unexpected behaviors.

One of the early experiments relating to QM's novel entanglement, probabilistic and deterministic behaviors began with the Einstein, Podolsky and Rosen (EPR) gedanken experiment [1]. This term meant that it was a thought experiment, and not conceived to be actualized, as position and momentum are not ideal for observing attributes very accurately. This tackled the problematic condition known as Heisenberg's uncertainty principle, wherein one could not measure both non-commuting properties of a particle, such as momentum and

position, at the same time! EPR, however, suggested a novel experimental configuration that, in theory, could allow the measurement of non-commuting properties! In its simplest form, two similar or identical particles, 1 and 2, fly off from a common location in opposite directions, thereby acquiring related physical properties. For example, one can measure the position of particle 1, and the momentum of particle 2. Owing to the symmetry of this hypothetical experiment, would allow both particles' non-commuting properties to be simultaneously determined! This method appears to work because the two identical particles serve as each other's mirror image twin. Thereby, one can gain information on both particles non-commuting properties! In Quantum Field Theory (QFT), electrons have structural differences depending upon whether the electrons are bound or free. Lindgren illustrates some of these differences via a QFT equation, shown in **Figure 1** [2]. Schatten and Jacobs outlined how virtual photons could play a role in the EPR conundrum [3].

2. Methods

We shall be basing our analysis of the electron's structure upon Quantum Field Theory's (QFT) picture of this as described by Lindgren [2]. **Figure 2** illustrates

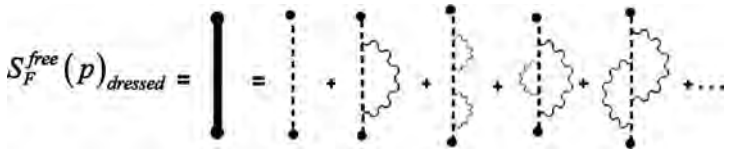

(1)

Figure 1. Shows a QFT equation that depicts the difference between a QFT bare electron and a QFT free electron, the latter being a "dressed" electron. A free electron, solid line at left, can be represented as the sum of a bare electron, dashed vertical line, plus its dressing, consisting of one or more virtual particles, shown by dashed semi-circles, towards the right, that the electron can withdraw from the vacuum, corresponding to the remainder of the equation.

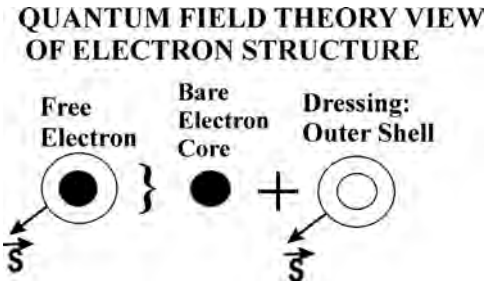

Figure 2. The physical structure of a free electron, corresponding to **Figure 1**'s equation is depicted. On the left the free electron is shown, consisting of a bare core plus an outer shell described in QFT as a "dressing". The bare core may be as small as a point defect in the divergence of the electric field or as large as the classical electron radius. Free electrons contain a dressing of one or more virtual particles drawn from the vacuum, garnered as they leave their bound state. Most commonly this consists of a virtual photon, having spin. When bound in atoms, electrons contain the electron core, plus three specific Pauli spin matrices. These provide several bits of information, little compared with the 3-D vector information associated with the virtual photons acquired into the free electron shell.

this via a simplified Quantum Field Theory (QFT) physical picture. It helps to bear in mind, that the Maxwell stress tensor consists of tension along the field, and pressure perpendicular to the electric field direction.

For charged particles, virtual photons, shown in the Feynman diagram of Figure 1, are the most common virtual particle. Figure 2 illustrates this via a physical picture that is based on the general Quantum Field Theory (QFT) view. We now consider the details of the Bohm version (B-EPR) of the Einstein, Podolsky, Rosen (EPR) experiment [1] [4]. This offers a more detailed account of free electron properties within the B-EPR experiment than is typically considered. Let us briefly describe how Stern-Gerlach Detectors (SGDs) work. Within these detectors, electrons are attached to neutral silver atoms to create a beam of neutral particles that pass through the SGDs. The SGDs have a strong magnetic field gradient in a direction perpendicular to the beam and detector axis. This field gradient provides a force in the direction of the field gradient, dependent upon the electron's spin in that direction. This separates the particles along the field gradient direction, by amounts dependent upon the spin component or components in that direction. Since electrons have spin 1/2 the beam splits up into two separate beams, spin UP and spin DOWN. This employs a single random vector (RV) via a random vector paradigm (RVP) to model each electron's dressing. For this paper, the usage allows free electrons a greater degree of determinism than the 3 sets of 2×2 Pauli spin matrices provides for tightly bound electrons. In the B-EPR experiment, the free electrons have their spin gauged by Stern-Gerlach (SG) detectors.

The free electron and positron, in Quantum Field Theory, contain one or more virtual particles in their dressings. These are typically virtual photons, drawn from the vacuum, serving to cloak these particles as they leave any strongly bound state. Like an evanescent electromagnetic field within a conductor, the field gradually diminishes with distance, inhibiting EM radiation. For the B-EPR experiment, the positron and electron leave their common zero-spin state, shown in Figure 3. For the purposes of the EPR experiment, when attached to a neutral atom, these particles behave similarly, allowing Stern-Gerlach Detectors (SGD) to sample their spin attributes. The only pre-condition set for the particles' spins is that the two particles contain oppositely oriented spin vectors, owing to the conservation rule associated with their zero-spin state origin, namely:

$$\vec{s}_E = -\vec{s}_P . \tag{2}$$

Equation (2) is, essentially, an "entanglement" equation, creating a bond or commonality that defines the two particles' co-existence, much as identical twins possess. We can refer to this as the B-EPR "spin entanglement equation". Other types of entanglement are also possible, dealing with a property that one system or particle possesses, having an attribute related to another's property. These generally may be considered as being the result of quantum "entanglement", a quantum condition that links the entities together, such as position and momentum, much as EPR originally considered. Namely, one particle can have its

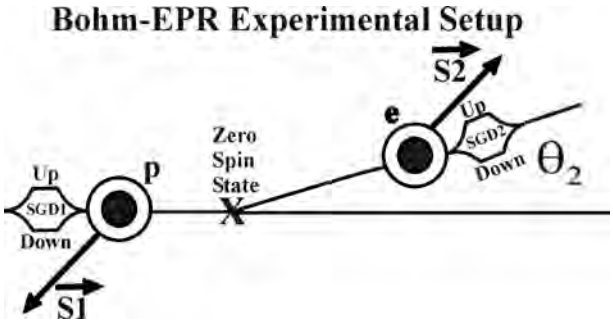

Figure 3. In the B-EPR experiment, a positron, p, particle 1, and an electron, e, particle 2, emanate from a Zero-Spin State located at **X**. The figure shows the particles' inherent structure, as having a bare core, surrounding which is a "dressing" containing one or more virtual particles (commonly a virtual photon). The two charged fermions: a positron, P = particle 1, and an electron, E = particle 2, exit their parturition site at **X**. Subsequently, they travel towards the Stern-Gerlach Detectors (see Feynman *et al.*) SGD1 and SGD2 [5]. These are oriented at relative angle, θ_2, with respect to each other. In the Random Vector Paradigm (RVP), each dressing contains an equal and opposite 3D random vector that provides connected spin information: $\vec{s}_E = -\vec{s}_P$, thereby creating a mathematical dependency, appearing as "quantum entanglement."

position measured, and its twin have its momentum measured, and thus obtain both properties for both particles simultaneously! Not often appreciated, is that free electrons can convey vector information in their dressings. The question of the locality of the information remains. In the B-EPR experiment, the particles appear non-locally related, owing to the distant locations from each other, when the two particles' spins are measured. This is an unfortunate conclusion, because the two particles originate from the common zero spin state at **X**; hence they are locally related.

At this point QFT's role ends, having supplied the dressed electron paradigm. From this, we hypothesized the sum of each particle's dressing can be expressed as a spin vector, which we refer to as the random vector paradigm (RVP), thereby allowing these fermions to possess 3D random vector spin information, which contains a significantly greater amount of information than is available from tightly bound electrons within an atom.

3. Results

To obtain the results, a computer generated simulation of the EPR experiment was carried out. Commonly, this is referred to as a "Monte Carlo" simulation. This term is chosen in particle physics because progress is made through numerical simulations of theory, using dice-like random number generations, rather than theoretical models to compare with experimental data. We use the random vector paradigm, RVP, to generate a Monte Carlo simulation, named Shimony, owing to his exuberance in spreading the interesting paradoxical aspects of the Bohm-EPR experiment. It is through our Monte Carlo simulation that we obtain our numerical results. For each point in the figure, 500 individual Bohm-EPR simulated electrons were passed through the numerical code, and the

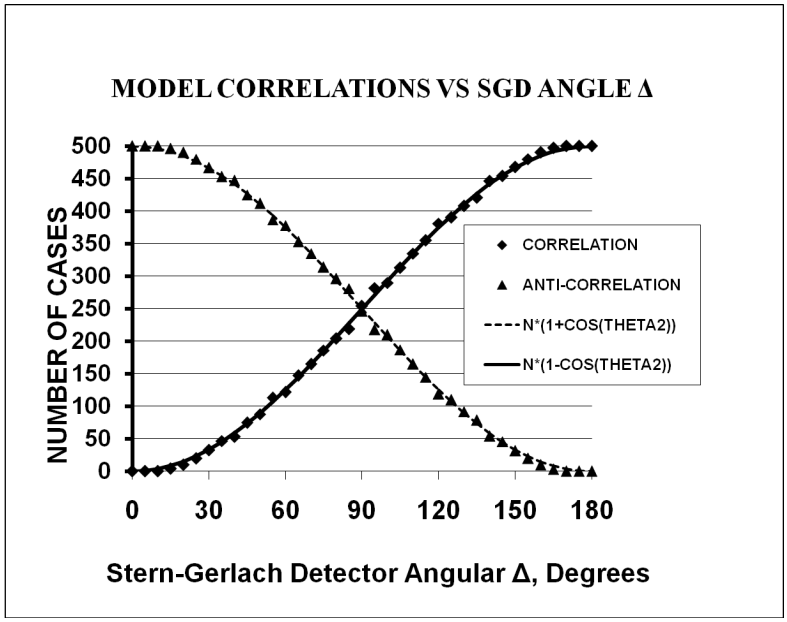

Figure 4. Correlations and Anti-Correlations in the B-EPR experiment (diamond and triangle points), compared with Bell's formulae (the solid and dashed curves). Positive correlation indicates the SGDs read + + or − −. Anti-correlation indicates opposite responses + − or − +. The abscissa indicates the relative angular orientation between the two Stern-Gerlach detectors. At an angle of 0˚ anti-correlations dominate; at 180˚ positive correlations exist; whereas at 90˚, stochastic behavior ensues: a puzzling tapestry of responses. Although there seems to be general agreement, these results only apply to a single EPR experimental setup. There are many other puzzling EPR experiments as well as non-EPR experiments.

results summed. For the case of positive correlations, each point added meant that either a + + or − − spin orientation was detected by the two Stern-Gerlach Detectors (SGD). Each anti-correlation point meant that either a + − or a − + SGD1 and SGD2 detector results occurred and then the sums were added up.

Figure 4, obtained from the Shimony algorithm, shows the correlations and anti-correlations in the model simulation, as the triangle and diamond sums, compared with Bell's formulae shown by the solid and dashed curves.

4. Discussion

The numerical correlations and anti-correlations compare well with Bell's summary of the B-EPR experimental form. Bell [6] found "non-local hidden variables" were involved to explain his findings. Despite our results being in accord with Bell's, we draw a somewhat different conclusion. We can agree with Bell's calling the spin properties of the two particles "hidden variables". We consider that the 3D spin vectors obtained by the free positron-electron pairs used in the experiment go beyond the normal atomic Pauli spin matrices. There is a difference in our understanding of the cause of the correlations found, however.

We agree that the two fermions cannot affect each other, owing to their separation, except "non-locally". Traditionally, locality in physics has been taken to indicate that an object is only influenced by local forces or particles, etc., as op-

posed to distant effects, often called "action at a distance". Still, our understanding of the experiment, is that it starts out at the same event, let us say, at T_0, when the positron electron pair were released from the Zero-Spin-State towards two different directions within the experiment, namely towards the two detectors. With the two particles having "entangled" spin vectors, the detectors each measure their respective spin vector "locally", associated with the interaction of the particle as it is observed by the detector through it locally sampling its spin vector.

It appears that non-locality in quantum mechanics has been accepted, as a strange quantum phenomenon that seemingly violates the special theory of relativity through the "spooky action at a distance". Essentially, the physics community has given a green light to non-locality in quantum mechanics, since everything else in QM is also so puzzling. In the B-EPR experiment, it is possible to observe particles 1 and 2 close enough in time, so that they have a spatial separation, not a temporal one. Hence, the two-particle observations appear not to be causally related, namely with a space-like interval between the two observations, one makes the assumption that neither can affect the other by direct influences. Then, when we see the observations are surprisingly correlated, this is taken to mean there is "spooky action at a distance", or non-local influences, or other words to that effect. It appears to this author, that since the experiment began at a time, say T_0, when the Zero-Spin-State released the two fermions, and later, both observations were temporally related to this time, $T_{0,}$. As a result the physics going on is best considered local, rather than non-local! One can easily fool ourselves into thinking that the measurement on one is affecting the other, whereas in reality, the properties of both were "caused" earlier at time, T_0. A correlation is NOT the same as causality. The data are correlated because they both arose from a common zero-spin-state, but neither one "causes" the other. They are simply mathematically linked, both "caused" by an event that branded both, earlier in time than either was observed, namely T_0. Hence both observations are "time-like" events associated with their common earlier origin at T_0. In this view, there appears to be a total absence of any "non-local, action at a distance, spooky" behaviors occurring within the B-EPR experiment.

This is not to say that the experiment is not a brilliant one, nor that further information cannot be gleaned by more sophisticated EPR and non-EPR experiments that may shed light on the correlations found, with further room for inventive geometries, timings, etc. Nevertheless, it does seem that, at least for the standard B-EPR experiment that Bell reported on, the observations seem to reveal valuable, interesting correlation forms that can really shed a great deal of light on how Quantum entanglement and probabilistic behaviors arise. Quantum Mechanical behaviors are really extraordinarily difficult to fathom, and most, particularly the B-EPR behaviors indeed are mostly counter intuitive. But the beautiful aspect of Quantum Mechanics, is that if one follows a good prescription, things do manage to get sorted out properly.

Beyond the results found here, there exists a panoply of other EPR-type experiments, as well as other non-EPR quantum puzzles that have totally different behaviors than the B-EPR one described here. Bohm referred to the QM puzzles with his viewpoint called "the Implicate Order", indicating some larger-scale order exists amidst the chaotic nature involved within these tiny bits of matter [4]. It is difficult to understand what David Bohm meant with this term. Yet he spent his lifetime considering quantum mechanics, and certainly entanglement is a major quantum component requiring understanding. To this author, it may indicate that he actually believed in determinism within physics much as Einstein did, however, probabilistic behaviors arise simply as a reflection of our inability to completely know all the "hidden variables" involved. With weather and climate forecasting, we now know that many systems behave "chaotically", not meaning a disparaging aspect of their behavior, but simply, in the mathematical sense, as a "sensitivity to initial conditions". None of this was known during most of the 20th century, so quantum's entanglement and probabilistic behaviors were doubly perplexing then. We now recognize that there are mathematical/physical limits beyond which one can never see into the future.

I shall add a few further thoughts about Quantum entanglement. It appears that entanglement is an immensely powerful controlling process, much as a rigid bridge can span distances and thereby reduce travel time. This is how the spin orientations of the two particles in the B-EPR experiment remain connected, despite even should vast distances separate the particles. Yet we also know that the two particles behave within the constraints of special relativity. However, because of the constraints that Quantum Mechanics imposes on particles, these connections have been suggested for a wide variety of uses in various diverse fields, such as computers, cybernetics, data encryption, theoretical physics, and many others. The current findings do NOT take away from the many possible ways that quantum phenomena can play in advanced computer systems, such as using Qubits, etc. Rather, the reverse is true, these experiments actually point more strongly to the fact that quantum correlations are powerful and can lead to 100% determinism if undertaken properly. Hence there are ways of achieving advanced data processing, well beyond the standard computer bits of 0 and 1. In quantum computers, using Qubits, the phases of the electromagnetic field can greatly expand the processing power using phase information, rather than just the limiting 1 standard bit of present day computers. This is a wide open field. Additionally, now that we may better understand how quantum entanglement works, there may be greater confidence in using these methods, particularly in encryption, data security, and simple data processing to enhance forecasting with greater accurate models.

Acknowledgements

The author was fortunate to have met Abner Shimony, who generously shared

his enlightened knowledge and deep understanding of many quantum puzzles, including the Bohm-Einstein, Podolsky, and Rosen experiment. The author also appreciates discussions with Sabatino Sofia, Verne Jacobs, and Hans Mayr.

Author Information

The author works for ai-Solutions, Inc., Lanham, MD USA.

Conflicts of Interest

The author declares no conflicts of interest regarding the publication of this paper.

References

[1] Einstein, A., Podolsky, B. and Rosen, N. (1935) *Physical Review*, **47**, 777-780. https://doi.org/10.1103/PhysRev.47.777

[2] Lindgren, I., *et al.* (1998) *Physical Review A*, **58**, 1001-1015. https://doi.org/10.1103/PhysRevA.58.1001

[3] Schatten, K. and Jacobs, V. (2020) *Canadian Journal of Physics*, **98**, 895-899. https://doi.org/10.1139/cjp-2019-0537

[4] Bohm, D. (1951) Quantum Theory. Prentice Hall, Englewood Cliffs.

[5] Feynman, R.F., Leighton, R.B. and Sands, M. (1965) Feynman Lecture Notes, II 35.1-6, III 6.1-6.14. Addison-Wesley, Reading.

[6] Bell, J.S. (1966) *Reviews of Modern Physics*, **38**, 447-452. https://doi.org/10.1103/RevModPhys.38.447

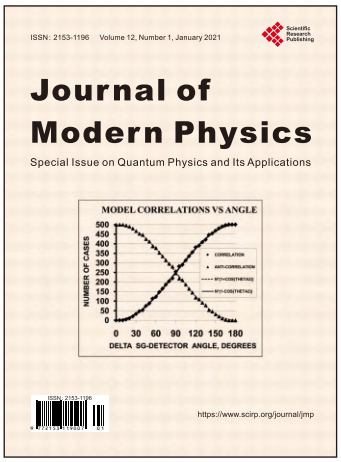

Call for Papers

Journal of Modern Physics

ISSN: 2153-1196 (Print) ISSN: 2153-120X (Online)
https://www.scirp.org/journal/jmp

Journal of Modern Physics **(JMP)** is an international journal dedicated to the latest advancement of modern physics. The goal of this journal is to provide a platform for scientists and academicians all over the world to promote, share, and discuss various new issues and developments in different areas of modern physics.

Editor-in-Chief

Prof. Yang-Hui He City University, UK

Subject Coverage

Journal of Modern Physics publishes original papers including but not limited to the following fields:

Biophysics and Medical Physics
Complex Systems Physics
Computational Physics
Condensed Matter Physics
Cosmology and Early Universe
Earth and Planetary Sciences
General Relativity
High Energy Astrophysics
High Energy/Accelerator Physics
Instrumentation and Measurement
Interdisciplinary Physics
Materials Sciences and Technology
Mathematical Physics
Mechanical Response of Solids and Structures
New Materials: Micro and Nano-Mechanics and Homogeneization
Non-Equilibrium Thermodynamics and Statistical Mechanics
Nuclear Science and Engineering
Optics
Physics of Nanostructures
Plasma Physics
Quantum Mechanical Developments
Quantum Theory
Relativistic Astrophysics
String Theory
Superconducting Physics
Theoretical High Energy Physics
Thermology

We are also interested in: 1) Short Reports—2-5 page papers where an author can either present an idea with theoretical background but has not yet completed the research needed for a complete paper or preliminary data; 2) Book Reviews—Comments and critiques.

Notes for Intending Authors

Submitted papers should not have been previously published nor be currently under consideration for publication elsewhere. Paper submission will be handled electronically through the website. All papers are refereed through a peer review process. For more details about the submissions, please access the website.

Website and E-Mail

https://www.scirp.org/journal/jmp **E-mail: jmp@scirp.org**

What is SCIRP?

Scientific Research Publishing (SCIRP) is one of the largest Open Access journal publishers. It is currently publishing more than 200 open access, online, peer-reviewed journals covering a wide range of academic disciplines. SCIRP serves the worldwide academic communities and contributes to the progress and application of science with its publication.

What is Open Access?

All original research papers published by SCIRP are made freely and permanently accessible online immediately upon publication. To be able to provide open access journals, SCIRP defrays operation costs from authors and subscription charges only for its printed version. Open access publishing allows an immediate, worldwide, barrier-free, open access to the full text of research papers, which is in the best interests of the scientific community.

- High visibility for maximum global exposure with open access publishing model
- Rigorous peer review of research papers
- Prompt faster publication with less cost
- Guaranteed targeted, multidisciplinary audience

Scientific Research Publishing

Website: https://www.scirp.org

Subscription: sub@scirp.org

Advertisement: service@scirp.org